DESIGN AND APPLICATION OF AN INTERMEDIATE STRAIN RATE MATERIALS TESTING DEVICE

ORTA GERİNİM HIZLARI İÇİN MALZEME TEST CİHAZI TASARIMI VE UYGULAMASI

MÜCAHİD FURKAN KELEŞ

PROF. DR. BORA YILDIRIM

Supervisor

Submitted to

Graduate School of Science and Engineering of Hacettepe University

as a Partial Fuilfillment to the Requirements

for the Award of the Degree of Master of Science

in Mechanical Engineering.

2024

ABSTRACT

DESIGN AND APPLICATION OF AN INTERMEDIATE STRAIN RATE MATERIALS TESTING DEVICE

Mücahid Furkan KELEŞ

Master of Science, Department of Mechanical Engineering

Supervisor: Prof. Dr. Bora YILDIRIM

March 2024, 50 pages

Intermediate strain rates are an interesting topic for many industrial sectors such as the automotive sector. Intermediate strain rates are important in the change of the material behavior and the material deformation process from low to high strain rates. However, due to experimental challenges, material characteristics at intermediate strain rates are rarely defined, creating a gap in the experimental data between low and high strain rates. One major challenge for experimental data in the intermediate strain rate region is the limitation of commercial load cells. Intermediate strain rate frequencies coincide with the natural frequency of these devices, which result in high noise. Therefore, new testing methods and experimental test data with intermediate strain rate loadings are required. In this study, an intermediate strain rate testing device is designed, produced and tested for three different materials: AA6061-T6, OFHC Copper and Polycarbonate. 3D Finite element simulations are conducted with LS – Dyna software for each material tests.

Experimental and numerical results are given and compared to numerical simulations and literature data. Comparison of numerical and experimental results showed a good match between simulations and experiments. Furthermore, experimental data compared to literature showed less than 10% error in all tests.

Keywords: Material Testing, Johnson – Cook Material Model, LS – DYNA, Split – Hopkinson Pressure Bar, Wave Separation, Intermediate Strain Rate

ÖZET

ORTA GERİNİM HIZLARINDA MALZEME TESTLERİ İÇİN TEST SİSTEMİ TASARIMI VE UYGULANMASI

Mücahid Furkan KELEŞ

Yüksek Lisans, Makine Mühendisliği Bölümü

Tez Danışmanı: Prof. Dr. Bora YILDIRIM

March 2024, 50 sayfa

Otomotiv sektörü başta olmak üzere orta gerinim hızları birçok endüstriyel sektör için önemli bir konudur. Orta gerinim hızları, yavaş gerinim hızlarından yüksek hızlara geçerken malzemenin davranışında ve deformasyonundaki değişim için önemlidir. Ancak, deneysel zorluklar nedeni ile orta gerinim hızlarında malzeme davranışı nadiren tanımlanır. Bu zorlukların temel nedeni orta gerinim hızlarında toplanması gereken veri frekanslarının ticari olarak satılan gerinim sensörleri tarafından doğru bir şekilde ölçülememesidir. Bu gerilim hızlarında görülen frekanslar gerinim ölçerlerin doğal frekansına yakındır ve bu nedenle veride gürültü çoğalır. Bu da yavaş ve hızlı gerinim hızları arasında bir boşluğa neden olur. Bu nedenle, orta gerinim hızlarında yeni test sistemleri ve deneysel veriye ihtiyaç vardır. Bu çalışmada, orta gerinim hızları için bir test sistemi tasarlandı, üretildi ve üç farklı malzeme ile test edildi: AA6061 – T6, OFHC – Bakır ve Polikarbonat. Her malzeme için 3 boyutlu sonlu eleman simülasyonu, LS-DYNA yazılımı ile yapıldı. Deneysel ve nümerik simülasyon sonuçları verildi ve literatür

ile karşılaştırıldı. Nümerik ve deneysel çalışmaların karşılaştırılması sonucunda iyi bir uyum görüldü. Deneysel testlerin literatür ile karşılaştırılmasında ise hata oranı her malzeme için %10'un altında bulundu.

Anahtar Kelimeler: Malzeme Testleri, Johnson – Cook Malzeme Modeli, LS-DYNA, Ayrık – Hopkinson Basınç Barı, Dalga Ayrıştırma, Orta Gerinim Hızı

ACKNOWLEDGEMENTS

Firstly, I would like to express my gratitude to my supervisor, Prof. Dr. Bora YILDIRIM for his guidance and assistance during my thesis studies.

I would like to thank the rest of my thesis committee members, Doç. Dr. Can Ulaş DOĞRUER, Doç. Dr. Mehmet Nurullah BALCI, Doç. Dr. Hasan Basri ULAŞ and Dr. Öğr. Üyesi Mehmet Okan GÖRTAN.

I would like to extend my sincere thanks to my colleagues and friends, Dr. Hakan HAFIZOĞLU, Ali Kürşat ATAY, Muzaffer Toprak, Onur EVCİ, İbrahim ŞAHİN and Ahmet İLERİ who helped and supported my thesis studies.

I would also like thank my supervisors in TUBİTAK SAGE, Dr. Hüseyin Emrah KONOKMAN and Mehmet Sarper YAVUZ who provided me with the opportunity and means to complete my thesis studies.

Finally, I would like to thank my beloved family; Naci KELEŞ, Gülay KELEŞ, Rıdvan KELEŞ and Meryem KELEŞ for their encouragement and belief in me.

Furkan KELEŞ

Nisan 2024, Ankara

TABLE OF CONTENTS

LIST OF FIGURES

LIST OF TABLES

SYMBOLS AND ABBREVIATIONS

Symbols

σ	Stress
ε	Strain
E	Young's Modulus
$\dot{\varepsilon}$	Strain rate
T	Temperature
K	Material coefficient
m	Material temperature softening coefficient
n	Material strain hardening coefficient
c	Material strain rate hardening coefficient
ε_t	Transmission bar strain
ε_i	Incident bar strain
c_b	Elastic wave velocity

Abbreviations

DBTT	**D**uctile to **B**rittle **T**ransition **T**emperature
PMMA	**P**oly (**m**ethyl **m**eth**a**crylate)
PC	**P**oly**c**arbonate
PTFE	**P**oly**t**etra**f**luoro**e**thylene
VISAR	**V**elocity **I**nterferometer **S**ystem for **A**ny **R**eflector
SHPB	**S**plit – **H**opkinson **P**ressure **B**ar
LLNL	**L**ivermore **S**oftware **T**echnology **C**orporation
AA6061-T6	**A**luminum **A**lloy 6061-T6
OFHC	**O**xygen **F**ree **H**igh **C**onductivity
CAD	**C**omputer **A**ided **D**esign
MPP	**M**assively **P**arallel **P**rocessing
GISSMO	**G**eneralized **I**ncremental **S**tress **S**tate Dependent Damage **Mo**del

1. INTRODUCTION

1.1. Strength of Materials

Strength of a material is often defined as the resistance of a material before it fails or plastically deforms. When a material is subjected to external loads, stresses and strains develop within the material due to internal forces in the material structure [1]. An example of a steel material under uniaxial tension loading is given in Figure 1.

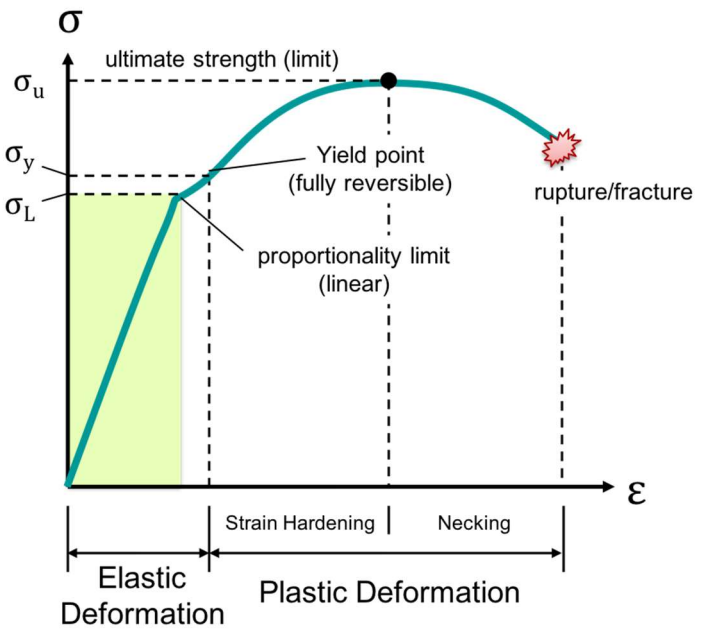

Figure 1: Example of a stress vs. strain graph [1].

In general, material response is examined under two main regions: elastic and plastic region. Yield strength of a material separates these two regions after which a material deforms plastically until fracture.

1.1.1. Elasticity

Elasticity works with elastic stresses and strains in materials. Elastic strength of materials can be explained with Hooke's Law which states that stress is directly proportional to strain and the elastic modulus of material. (See Equation 1)

$$\sigma = E\varepsilon \tag{1}$$

Hooke's Law is valid in stress vs. stress curve region before the proportionality limit. Where **σ** is the stress, E is the modulus of elasticity and **ε** is the strain.

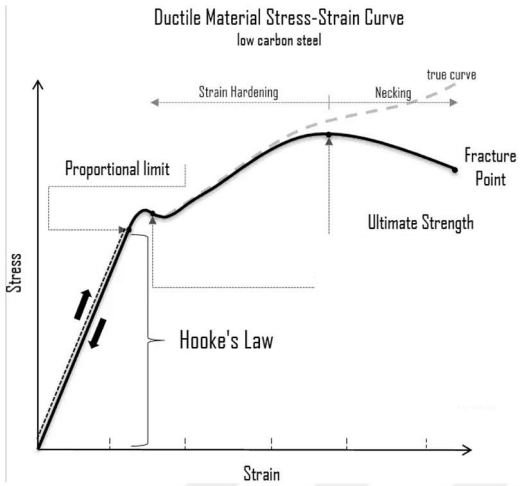

Figure 2: Example of a stress vs. strain graph for low carbon steel showing Hooke's Law [2].

1.1.2. Plasticity

Plasticity investigates material behavior after yielding. Response of material to external loadings in plastic region is harder to predict than elastic region due to effects such as strain hardening, temperature softening, necking, crack propagation, etc. An example can be seen in Figure 3, which depicts stress vs. strain curves for AISI 1040 steel material with different heat treatments. It can be seen that response of material in plastic region changes dramatically [3].

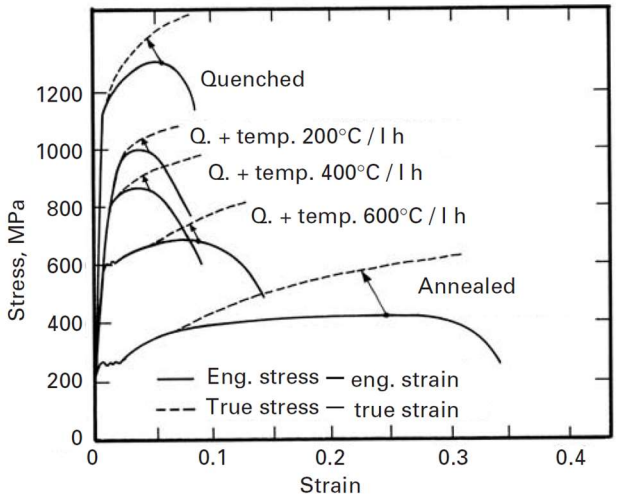

Figure 3: Stress vs. strain graphs for AISI 1040 steel with different heat treatments [3].

In order to predict plastic response of materials, different equations are used. One of the most commonly known equations is the Ludwik – Holloman equation which represents the stress – strain relation in polycrystalline metals [3]:

$$\sigma = \sigma_0 + K\varepsilon^n \tag{2}$$

Where exponent n is called the work-hardening coefficient and K is a constant depending on the material. Another equation was created by Voce, which uses empirical parameters to represent the relationship between stress and strain [3]:

$$\frac{\sigma_s - \sigma}{\sigma_s - \sigma_0} = \exp\left(-\frac{\varepsilon}{\varepsilon_c}\right) \tag{3}$$

Where σ_s, σ_0 and ε_c are empirical parameters depending on material, temperature and strain rate. There are many other equations used to determine the plastic response of materials such as Zerilli – Armstrong and Material Threshold Stress equations. However, the most known and commonly implemented in finite element analysis codes is the Johnson – Cook equation [4].

$$\sigma = (\sigma_0 + K\varepsilon^n)\left(1 + C\ln\frac{\dot{\varepsilon}}{\dot{\varepsilon_0}}\right)\left[\left(1 - \frac{T - T_r}{T_m - T_r}\right)^m\right] \tag{4}$$

Where σ_0 is the initial yield strength and K, n, C, m are material parameters representing strain hardening, strain rate hardening and temperature softening. $\dot{\varepsilon}$ is the strain rate, $\dot{\varepsilon_0}$ is the reference strain rate, T_m is the melting temperature and T_r is the reference temperature. An example of the Johnson – Cook representation of the plastic response can be seen in Figure 4.

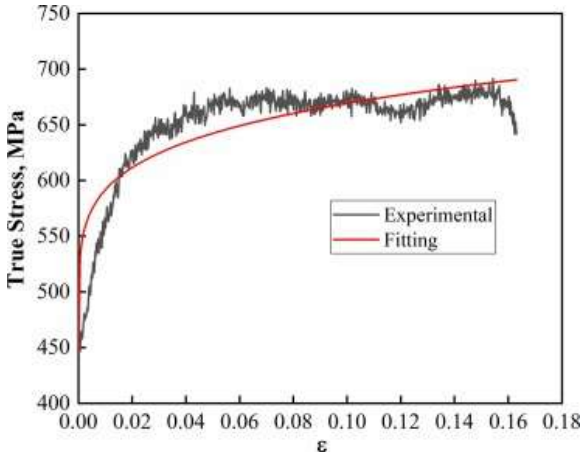

Figure 4: Johnson – Cook equation representation of plastic response and experimental data [5].

1.1.3. Strain Rate Hardening

Most materials show strain rate dependent mechanical behavior. Strain rate dependence of metals has been studied extensively for fifty years. One of the first studies about the strain rate dependent behavior of metals was conducted by Kolsky [6]. In his studies, he designed Kolsky Bar testing system which is now a commonly used dynamic testing system. Strain rate dependent behavior of metals is still an active research topic due to increased studies about ballistic impact dynamics.

Metals under high strain rates generally show different deformation and fracture compared to low strain rate loadings. One effect of high strain rates on metals is called strain rate hardening. Strain rate hardening causes metals to become stiffer. Although, this effect is almost negligible until high strain rates (10^2 s^{-1}), it becomes very significant under very high strain rates (10^5 s^{-1}) [7]. Effect of strain rate to material strength is visualized below in Figure 5.

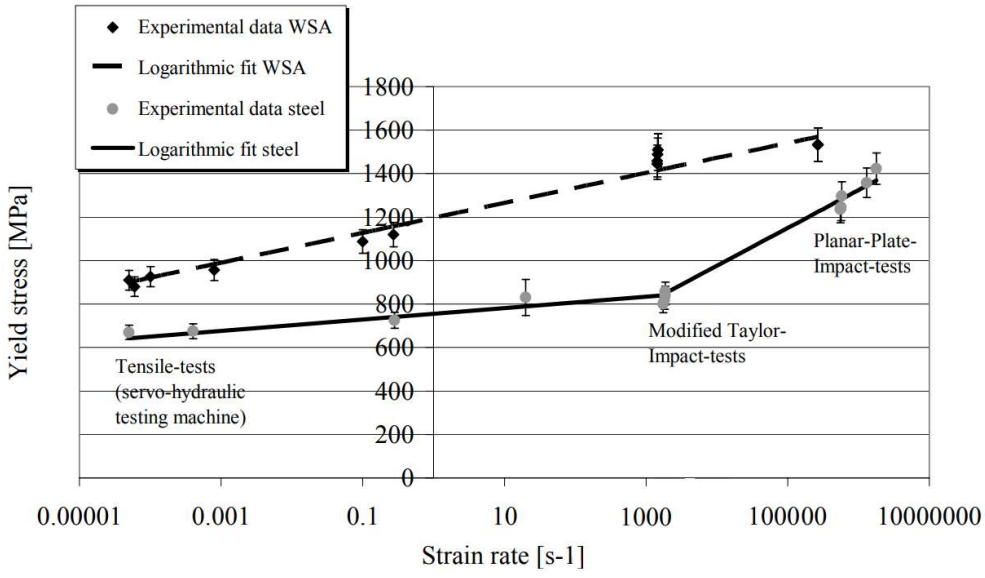

Figure 5: Effect of strain rate hardening on steel yield stress [7].

As it is seen on Figure 5, steels show increased yield stress with increasing strain rates. This effect is small under 10^3 s^{-1} strain rates but there is a sharp increase of strain rate hardening after an inflection point around 10^3 s^{-1}. This region of increased strain rate hardening depends on material type.

Similar results have been published for some engineering polymers such as PMMA and Polycarbonate [8]. Figure 6 below, shows results of quasistatic and dynamic tests on PMMA and PC materials.

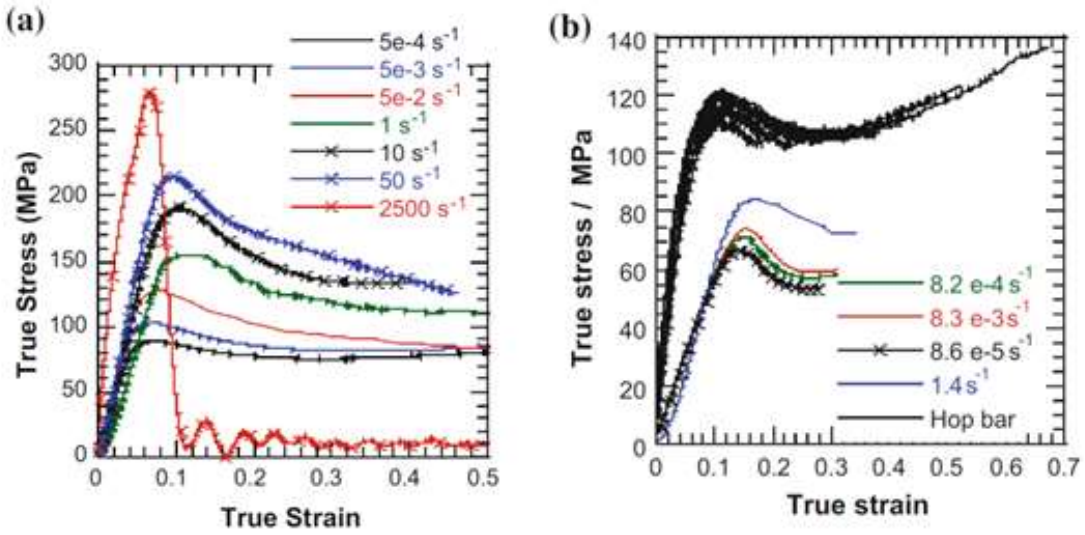

Figure 6: Compressive stress vs. strain graphs two polymeric materials. A: PMMA, B: Polycarbonate [8].

Glassy amorphous polymers such as polycarbonate and PMMA shows strain rate hardening under intermediate to high strain rates. Such polymers show a sharp increase of strain hardening in intermediate strain rates (10^0 s^{-1} – 10^2 s^{-1}) [8].

Strain rate dependence of materials not only effects material strength but material failures modes as well. An extensively researched property of metals is the ductile to brittle transition temperature (DBTT). Metals that are ductile under normal conditions show ductile failure properties under lower temperatures. Similar to this, ductile materials show highly brittle failure behavior under high strain rates. Another important aspect of strain rate dependence for material failure is the adiabatic shear bands. Adiabatic shear bands are usually seen in metals that are under high strain rates [9].

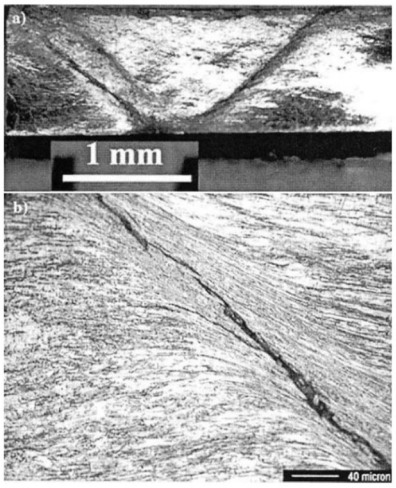

Figure 7: Adiabatic shear bands seen in tungsten alloys. A: adiabatic shear bands after dynamic compression test, B: polished and etched shear band [9].

1.2. Materials Testing

In order to uncover model material plasticity and failure behavior in numerical simulations extensive tests must be done. Generally, many different types of tests are required to completely simulate a material using a common material model such as the Johnson – Cook material model. Some of the most used materials testing methods are quasistatic uniaxial tension tests, high temperature tension tests, dynamic compression and tension tests, Taylor impact tests and plate impact tests [3]. Figure 8 shows some of these different testing methods for different strain rates. Materials testing methods can be categorized in two main groups: quasistatic materials testing and dynamic materials testing.

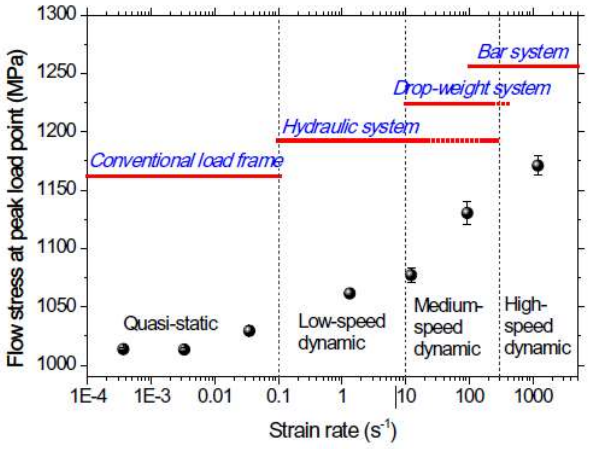

Figure 8: Material testing systems for different strain rates [10].

1.2.1. Quasistatic Testing

This is the most commonly used materials testing method to understand fundamental material response such as modulus of elasticity, yield strength, ultimate tensile strength and failure strain. In this method, an actuator is used with a load cell that captures forces acting on the specimen and an extensometer that records material deformation [11]. Schematic of a universal materials testing system can be seen below in Figure 9.

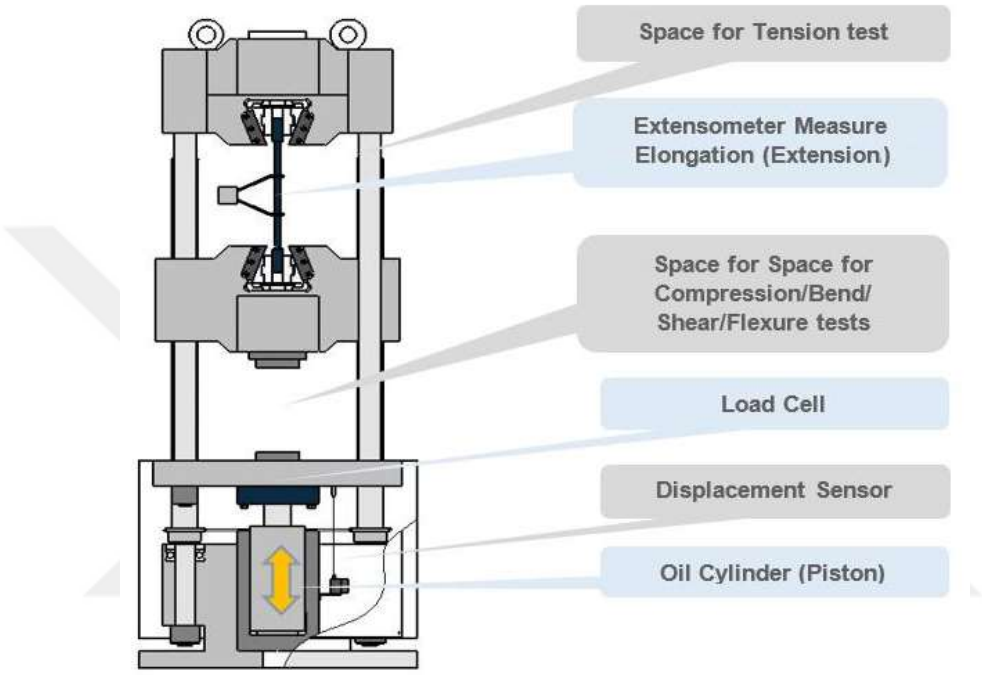

Figure 9: Schematic of a universal testing system [11].

Depending on the properties of the testing system, different deformation speeds can be chosen. This is achieved by changing the crosshead speed. Crosshead is the speed of the fixture that is connected to the specimen. Generally, crosshead speed range for standard systems are between 0.001 mm / min and 1000 mm / min. Some specialized high speed testing systems that use hydraulic servo actuators can reach crosshead speeds of 20 m/s [12]. Schematic of a high-speed testing system is given in Figure 9.

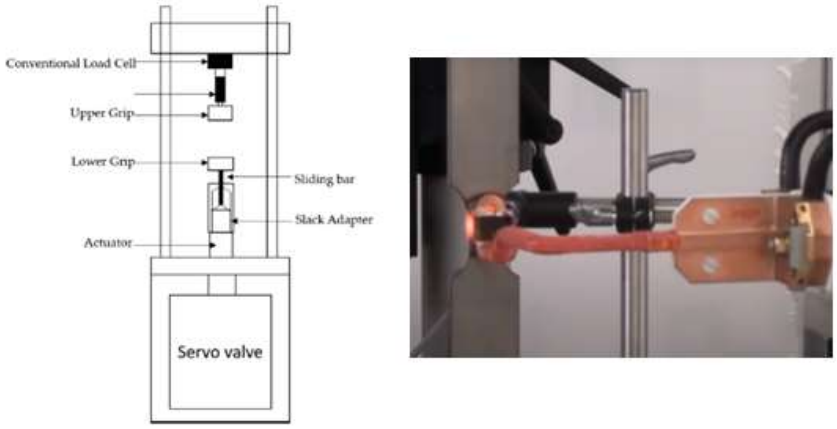

Figure 10: Schematic of a high–speed testing system and high–temperature testing [3].

Universal testing systems can also be equipped with a high – temperature testing equipment. This allows them to heat up the tested specimen before testing to observe temperature softening or other related material properties. Such a system is shown in Figure 10.

Furthermore, there many specimen types that can be used with a universal testing system. Different shaped specimens are used to observe materials' strength and failure properties under different loads. Some of these specimen types are [13]:

- Uniaxial tension specimens,
- Uniaxial compression specimens,
- Notched and pre-damaged specimens,
- Shear compressive specimens.

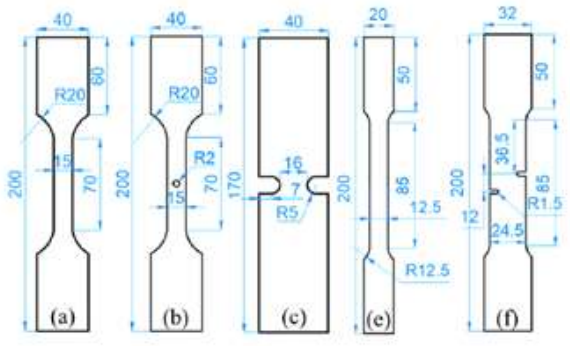

Figure 11: Standard tensile specimen, central-hole specimen, notched tensile specimen, tensile specimen, notched tensile specimen [13].

In Figure 11, different specimen types designed to explore material's failure behavior can be seen.

Universal testing systems use load cells to measure forces on the specimen. Load cells are piezoelectric devices that can transform forces to electric signals [14]. Load cell measurements are generally accurate up to strain rates 1 s^{-1}. This is due to the natural frequency of load cells [10]. There have been studies exploring custom – made load cells that can measure faster deformations speeds accurately. Xia et al. conducted various tests with a high – speed hydraulic servo testing system to design a custom – made load cell which reduced vibrations and allowed accurate measurement of forces [10]. Tests were conducted under 10 s^{-1}, 100 s^{-1} and 200 s^{-1} strain rates and accurate results are reported. These can be seen in Figure 12. However, these load cells are not commercially available.

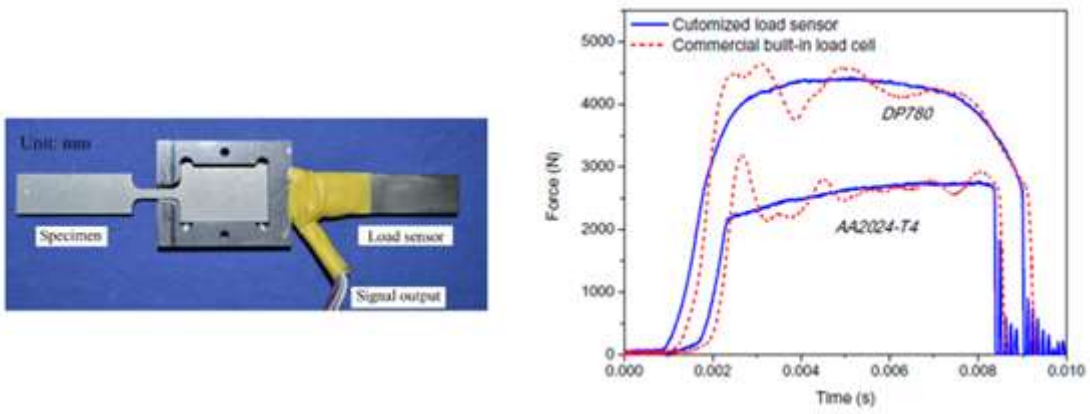

Figure 12: Customized load – cell and results by Xia et al. [10].

Universal testing systems use extensometers to measure the deformation of the specimen. There two main categories of extensometers: mechanical extensometers and video extensometers. Mechanical extensometers measure displacements by physically sensing the movement of the specimen and video extensometers use digital image correlation [15]. Using force data obtained from the load cell and displacement data from the extensometer, stress vs. strain curves can be obtained with this testing method.

1.2.2. Dynamic Testing

Materials show different thermomechanical behavior under dynamic loads and in order to understand this behavior many different dynamic testing methods are used. Some of the best-known tests are: Taylor impact tests, plate impact test and split – Hopkinson pressure bar tests [3].

Taylor impact tests are conducted by impacting a cylindrically – shaped specimen onto a rigid plate. Taylor impact tests are designed and first used by Taylor in 1948 as a low – cost, high impact energy test that also has good repeatability [3]. Taylor impact tests are used to obtain dynamic yield stress of the material by measuring the final dimensions of the specimen. Depending on the shape of the final state, dynamic strength properties of the material is determined [16]. Figure 13 shows a schematic of the test and an example of the final specimen shape.

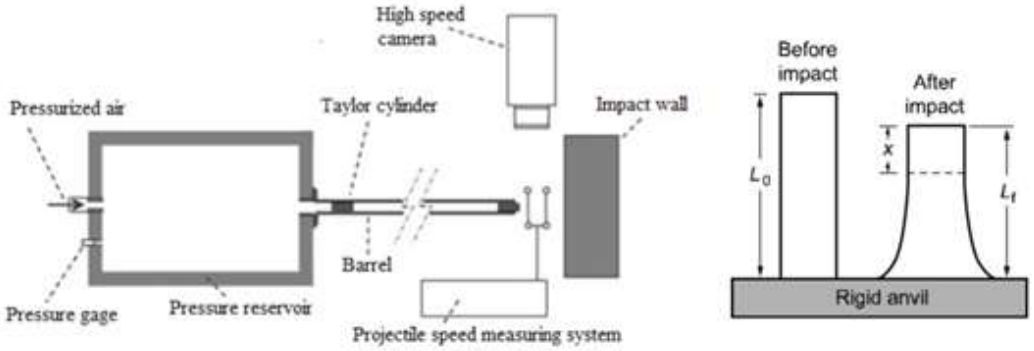

Figure 13: Schematic of Taylor – impact test and specimen shape before and after testing [17] [16].

Plate Impact tests are similar in principle to Taylor impact tests. Plate impact tests use plate specimens instead of slender cylinders to achieve higher strain rates in the specimen. In plate impact tests, specimen is mounted and remains static while a rigid projectile is accelerated using generally a gas gun. When the projectile impacts the specimen a uniaxial – strain state is obtained in the specimen due to its plate shape. Effects of this state and very high strain rates ($>10^5$ s^{-1}) achieved during the test is generally recorded using a "velocity interferometer system for any reflector (VISAR)". VISAR measurement system can obtain velocities at very high frequencies at a point on the specimen. To obtain the velocity values for the impacted specimen, probes are mounted on the back side of the specimen. These probes are connected to VISAR system which records the velocity profile during the test with an oscilloscope. Velocity profile obtained with VISAR can be used to calculate yield stress, strain and strain rates. Furthermore, data about the spall resistance of the material can also be obtained with plate impact testing. Figure 14 shows a schematic of plate impact test and an example of velocity profile obtained with VISAR [7].

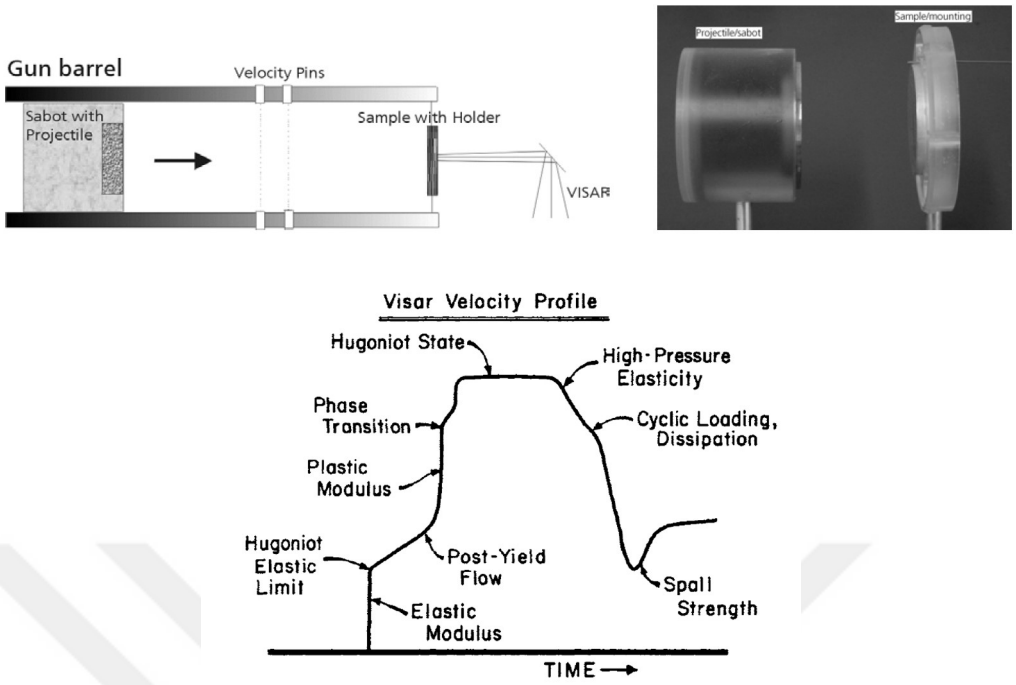

Figure 14: Example of a plate impact test setup and VISAR velocity profile with material properties [3] [7].

Split – Hopkinson pressure bar tests are very common for dynamic materials testing. While Taylor impact and plate impact tests obtained material data indirectly, split – Hopkinson pressure bar testing method can obtain stress vs. strain curves directly from the specimen. It is also very straightforward and studied extensively by many researchers over the last fifty years [18].

Split – Hopkinson pressure bar test systems can be used similar to universal testing systems to obtain compression, tension, shear or failure data of the material. This is achieved by changing the specimen shape and the testing setup from compression to tension [18]. An example of a split – Hopkinson pressure bar system for compression testing schematic is given in Figure 15.

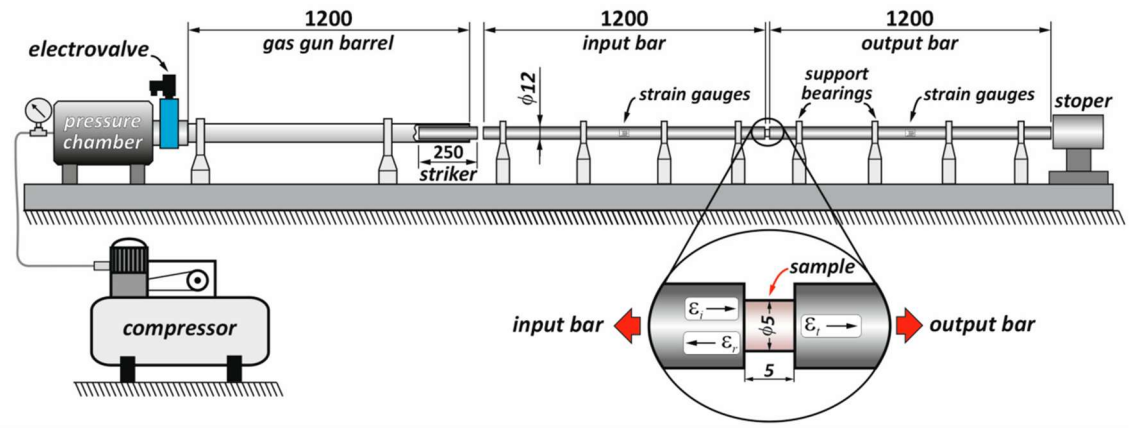

Figure 15: Split – Hopkinson Pressure Bar compression test system [19].

Split – Hopkinson pressure bar (SHPB) system consists of a gas gun, three slender bars generally made up of high strength steel and a cylindrical specimen. Gas gun is used to accelerate the striker bar which impacts with the incident bar. This impact generates a compression wave travelling across the incident bar, this wave is called the incident wave. Specimen is put between incident and transmission bars. Incident wave deforms the specimen and continues to propagate through the transmission bar while a reflection wave propagates backwards through the incident bar. There are two strain gauges cemented to incident and transmission bars, and these strain gauges capture incident, transmission and reflected waves. Strain histories of these waves are used to calculate stress, strain and strain-rate histories of the specimen according to the given formulas below [18].

$$\varepsilon(t) = -\frac{2c_b}{L}\int_0^t \varepsilon_r(t)\,dt \tag{5}$$

$$\sigma(t) = \frac{A_b E}{A_s}\varepsilon_t(t) \tag{6}$$

$$\dot{\varepsilon}(t) = -\frac{2c_b}{L}\varepsilon_r(t) \tag{7}$$

where: L, As are the length and the cross-section area of the specimen; E, A_b, c_b are the Young's modulus, the cross-sectional area, and the elastic wave velocity of the pressure bar, respectively [18].

Split – Hopkinson pressure bar system is generally used for dynamic materials testing between strain rates 10^2 s^{-1} and 10^4 s^{-1}. However, there have been studies about achieving

lower or higher strain rates with modified split – Hopkinson pressure bar systems. One of such modifications is the miniature Hopkinson bar (See Figure 16). Miniature Hopkinson bar can achieve higher strain rates (10^4 s^{-1} – 10^5 s^{-1}) [18]. This is achieved by reducing the diameter of the bars which allows one to use smaller specimens, therefore achieving higher strain rates. Another modification is the long Hopkinson bars. Long Hopkinson bar can achieve lower strain rates than a standard Hopkinson bar. This is due to increased test time achieved by increasing the length of the transmission bar [18].

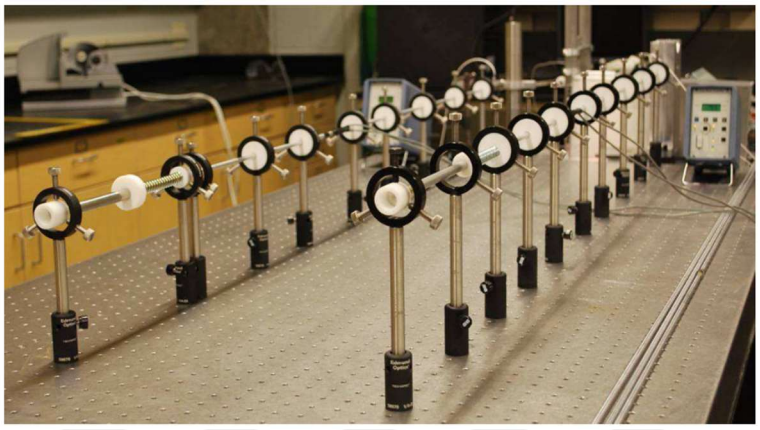

Figure 16: Miniaturized split – Hopkinson tension bars [18].

1.2.3. Intermediate Strain Rate Testing

In order deliver experimental data for materials used in engineering, a variety of techniques have been proposed to fill the hole between quasi-static and high strain rate testing. One option to conduct experiments with an intermediate strain rate regime was to use servo-hydraulic machines. Nevertheless, the accuracy of the test results is not particularly high. The issue is that high inertia throughout the experiment affects stress-strain data, and recordings made from these kinds of devices are frequently noisy and exhibit significant oscillations. Consequently, only strain rates lower than 10 s^{-1} may be reliably measured by servo-hydraulic devices [11].

Following the invention of the split – Hopkinson bar technology, a few researchers attempted to alter the traditional dynamic split Hopkinson pressure bar device in order to increase the loading time and produce a deformation rate in the intermediate rate domain. The test's time being constrained by the bars' length is the primary disadvantage of the altered apparatus, though. The specimen cannot develop a considerable strain at medium strain rates for such a time. Consequently, a different loading method needs to be used. In the past ten years,

some researchers have created specialized test apparatuses that can conduct intermediate strain rate tests to investigate material characterization. These include commercial machines created by companies like Instron and Shimadzu, as well as elastic-bar-type systems, modified servo-hydraulic load frames, drop tower and flywheel device [11].

1.2.3.1. Drop Tower

Drop tower tests are conducted by dropping a mass onto a structural component. Drop tower device is commonly used to analyze the behavior of the material as it crushes and collapses. Its primary application is in medium strain rate testing. Very little work has been done recently to create specialized equipment and technologies that would enable drop towers to conduct testing under varied weights utilizing precise load measurement methods like the Hopkinson bar technique or unique piezoelectric load cell. Bo Song and his associates created the "Dropkinson" bar, a novel tensile testing tool that can test at an intermediate strain rate, in 2018. The gadget was inspired by the drop tower [20].

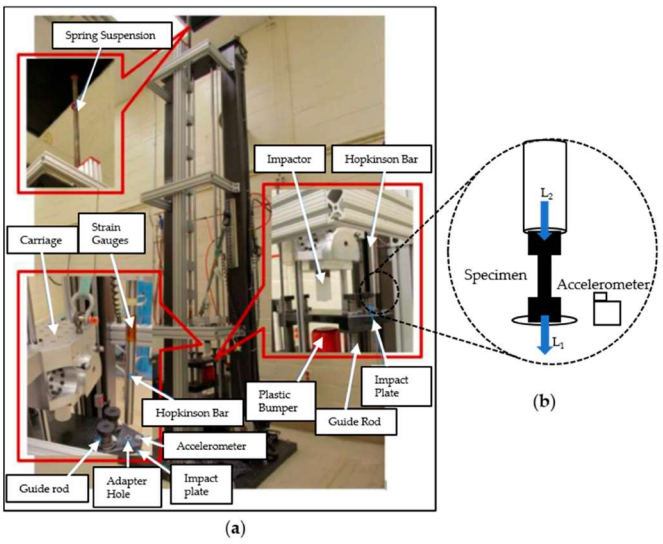

Figure 17: Dropkinson bar setup and specimen used in Dropkinson bar method [20].

The Dropkinson bar loading mechanism is a combination of a Hopkinson bar and a drop table that produces a consistent strain rate while facilitating steady and long-lasting impact velocity and specimen deformation. To lessen the impact of inertia in the system, the load history was measured using a lengthy Hopkinson bar system. The drop table and the Hopkinson bar are fastened in parallel. As seen in Figure 17, the trolley's free fall impact is produced using the drop table. During the test, the impact plate's center is struck by a cylindrical steel impactor that is fastened to the bottom of a carriage [20].

Following the carriage's free fall, the impactor attached to the carriage's bottom collides with the impact plate in the middle. The impact plate transmits the impact load to the tensile specimen under dynamic tension. The tensile stress wave enters the vertical bar via the specimen and bar end. The strain gauges affixed to the bar record the specimen's load history. A special laser extensometer is also employed to calculate the specimen strain. The newly designed Dropkinson bar has produced consistent results. However, there is substantial ringing noise, which may affect the force and strain readings as a result of the hit between the impactor and the moving metallic carriage [20].

1.2.3.2. Modified Kolsky Bar Test Method

Hybrid methods with modified servo – hydraulic load frame is another important system used in intermediate strain rate testing. LeBlanc et al. developed and introduced a new hybrid testing equipment in 1996 to perform intermediate strain rate tests to enhance the load measurement data obtained in high-speed servo hydraulic machines [21]. A servo-hydraulic machine was combined with the split Hopkinson bar technology to create this device. The device combines the loading capabilities of a servo-hydraulic testing machine with a Hopkinson bar load measurement approach. Othman conducted an experiment using a typical servo-hydraulic machine with a maximum speed of 16 m/s [22]. A steel bar with a length of 820 mm is fastened to the machine's upper crosshead. The strain gauges are connected to the bar. These gage placements enable for effective signal deconvolution. The specimen is connected to the bar as well as the lower crosshead. The high-speed video camera is set up in position so that the displacement field may be captured using the digital image correlation approach [23] [24].

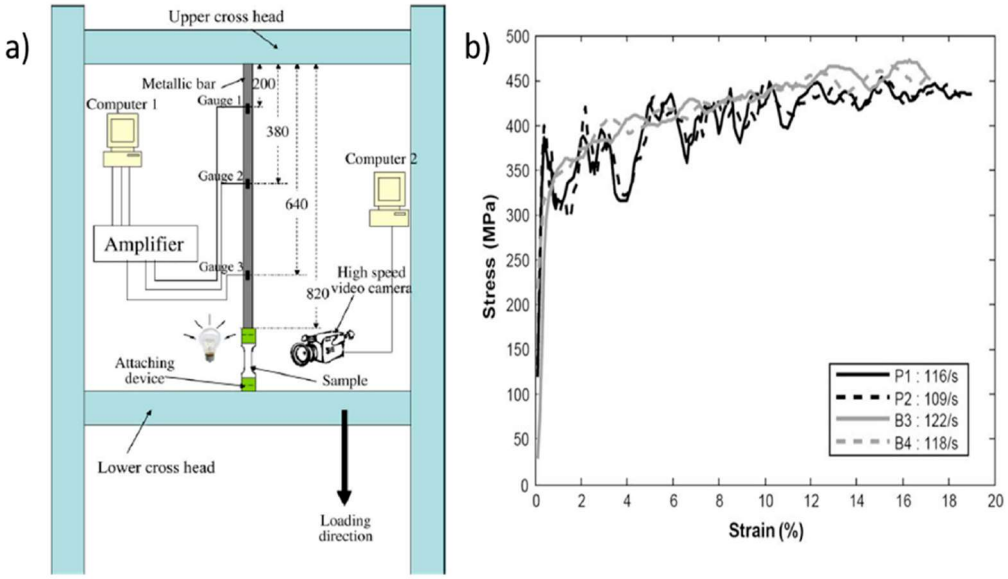

Figure 18: a) Modified Hopkinson bar device, b) stress vs. strain results using piezoelectric load cells (P1,P2) and Hopkinson bar method (B3,B4) [22].

The load sensors and Hopkinson bar approach are used to record the load records, and Figure 18 compares the stress-strain curves obtained from the two methods. Comparing the stress curve obtained with the Hopkinson bar method with that obtained with a piezoelectric load sensor, significant oscillations are seen. Stress waves, including reflected waves, are what creates the oscillations in the piezoelectric load sensor [10]. These studies show that, as compared to the conventional load cell, the hybrid test approach greatly enhances the quality of stress-strain test results. At an intermediate strain rate of around 100 s^{-1}, this novel Hopkinson bar approach for measuring the load exhibits less fluctuating behavior.

One benefit of using a hybrid testing device is that it provides more accurate stress-strain data since it exerts a continuous force during the test. By utilizing the strain gage that is fastened to the bar, the load may be calculated directly. Due to the particular length of the bar, the test's loading period was limited to 1 ms, which does not provide the specimen with enough strain. Additionally, Othman et al. altered the hybrid testing equipment to enhance the load measurement method by extending the test duration and utilizing the "wave separation method" to conduct the test at different strain rate regimes [22].

After an extensive literature survey, the most effective method for intermediate strain rate materials testing is found to be the hybrid method designed by LeBlanc and improved by Othman et al [22]. In this study, a modified servo – electromechanic Hopkinson bar system

is designed, manufactured and tested using their previous research. Aim, of this study is to be able to create an intermediate strain rate materials testing system with accurate and repeatable results.

1.2.3.3. Wave Separation Techniques

In conventional Hopkinson bar, strain rate is limited to high values dues to its limit on loading time. Formula for loading time and maximum strain in material is given in (8 below [25].

$$\text{Loading Time} = \frac{L}{2C} \tag{8}$$

Where L is the length of the Hopkinson bar and C is the speed of sound for Hopkinson bar. Stress wave travelling in the Hopkinson bar reflects from its end and when this reflected wave reaches the strain gauges used for stress measurement data becomes unusable. Therefore, wave separation methods are devised to overcome this challenge.

The effects of any number of separate waves can be distinguished from one another using wave separation techniques, which include processing at least two data, using mathematical tools. Lundberg, Henchoz, and Yanagihara implemented it to the Kolsky bar for the first time [26] [27]. The test time constraint brought about by the waves' overlap in strain gauge cross-sections is solved by the application of wave separation techniques. Either the frequency expressions or the temporal expressions of waves serve as the foundation for wave separation approaches [25].

The elementary wave theory of thin elastic rods served as the foundation for the development of the time domain wave separation techniques. Specifically, each cross-section of the bar's displacement may be expressed as the superposition of two waves traveling in opposite directions but at the same constant speed [25].

$$u(x,t) = f\left(t - \frac{x}{c}\right) + g(t + \frac{x}{c}) \tag{9}$$

where c is the sound speed, f is the displacement caused by the incident wave, g is the displacement caused by the reflected wave, and x is the cross-section location and t is time.

Lundberg, Henchoz and Yanagihara proposed to use two strain gauges on the bar to calculate the force and velocity at the specimen – bar interface. With the assumption that bar is slender and elastic, they have formulated strain and velocity as follows [26] [27]:

$$\varepsilon_0(t) = \varepsilon_0(t - 2T) + \varepsilon_0(t + T_1) - \varepsilon_1(t + T_1 - 2T_2) + \varepsilon_2(t - T_2) - \varepsilon_1(t - T_2 + 2T_1) \quad (10)$$

$$\frac{v_0(t)}{c} = \frac{v_0(t - 2T)}{c} - \varepsilon_1(t + T_1) - \varepsilon_1(t + T_1 - 2T_2) + \varepsilon_2(t - T_2) + \varepsilon_1(t - T_2 + 2T_1) \quad (11)$$

Where $\varepsilon_0(t)$ and $v_0(t)$ are strain and velocity at specimen – bar interface. T_1 is the wave arrival time to the first strain gauge. Similarly, T_2 is the wave arrival time to second strain gauge. T is the time difference between T_1 and T_2 [25].

Using this method, velocity and strain can be measured after the reflected wave passes strain gauges. This allows for infinite loading time since measurement is no longer a concern. However, there are some points to note when using this method [25]:

- This model is based on 1D wave propagation theory in slender bars; therefore, wave dispersion is neglected.
- This wave separation method is sensitive to noise in strain gauge measurements and errors on strain gauge locations.

In order to solve the problem of noise generation in this model, Jacquelin and Hamelin proposed a new method using three strain gauge readings and one velocity measurement at any strain gauge position of the bar [28].

Building on the Lundberg and Henchoz model (see Equation (9)), Jacquelin and Hamelin examined frequency domain calculations of the incident and reflected waves. They used Fourier's transform to Equation (10) and obtained the following frequency domain formula:

$$E_0(\omega) = \frac{E_A(\omega)\, sin(\omega T_B) - E_B(\omega)\, sin(\omega T_A)}{sin(\omega T)} \quad (12)$$

Where $E_i(\omega)$ is the Fourier transform of $\epsilon_i(t)$.

Denominator of equation (12) becomes zero at the frequencies shown in equation (13, this was remarked by different authors [28].

$$f_k = \frac{k}{2T} \quad (13)$$

This meant that at certain frequencies the equation is not defined. Technique of Lundberg and Henchoz cannot solve for strain data at certain frequencies. Jacquelin and Hamelin

discussed that this limitation is a function of the location of strain gauges and rewrote the equation as follows:

$$f_k^{A,B} = \frac{c(f_k)}{2(x_B - x_A)} \tag{14}$$

Where x_A and x_B are the strain gauge locations.

According to this method, it can be seen that a third "well – positioned" point for strain measurement can be chosen so that there is always a pair of points which will allow the determination of the equation 14 at all frequencies. When there are three points for strain data, three different pairs of measurement can be calculated [28]:

$$\begin{gathered} \epsilon_A(t) - \epsilon_B(t) \\ \epsilon_A(t) - \epsilon_C(t) \\ \epsilon_B(t) - \epsilon_C(t) \end{gathered} \tag{15}$$

Where $\epsilon_A(t)$, $\epsilon_B(t)$, $\epsilon_C(t)$ are three different strain measurements.

Jacquelin and Hamelin determined that the position for the third measurement point is given by the following equation:

$$x_C - x_B = x_A - x_0 \tag{16}$$

Proposed locations of the three points and the characteristic wave diagram for this is shown in Figure 19.

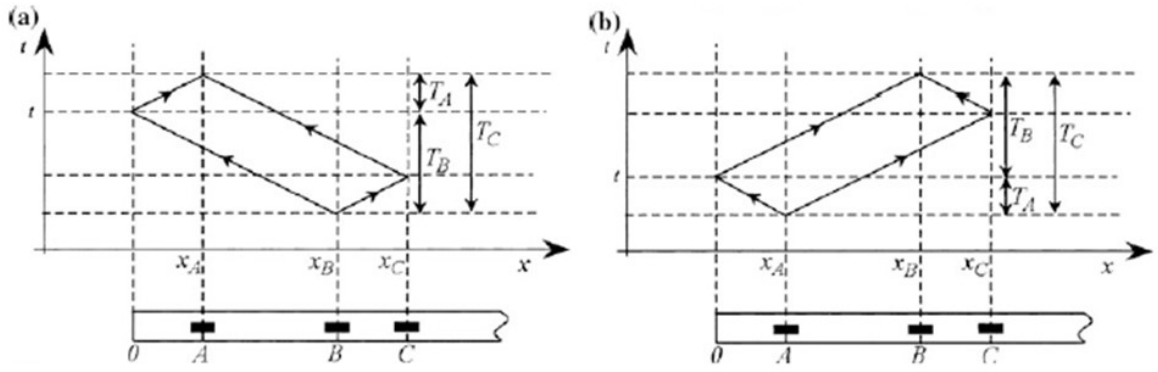

Figure 19: Characteristic wave diagram for an elastic bar with three strain gauges. A) depicts the incident wave, B) depicts the reflected wave [28].

Using the characteristic diagram for waves in Figure 19 it is possible to formulate the relation between strain measurements and strain at x = 0 as [25]:

$$\varepsilon_0(t) = \varepsilon(x_1, t + T_1) + \varepsilon(x_2, t - T_2) - \varepsilon(x_3, t + T_1 - T_2) \tag{17}$$

And velocity at x=0 as:

$$\frac{v_0(t)}{c} = -\varepsilon(x_1, t + T_1) + \varepsilon(x_2, t - T_2) - \frac{v(x_3, t + T_1 - T_2)}{c} \tag{18}$$

Method of Jacquelin and Hamelin solves the noise problem of the previous model [29]. However, it uses a velocity measurement at a strain gauge position for velocity at x=0. Such velocity measurements (Photon Doppler Velocimeter) are very hard to implement and are rarely used in Hopkinson bar systems [30].

Other wave separation methods which use frequency domain calculations aim to include wave dispersion effects and derive wave separation methods that can work with viscoelastic bars that have high wave dispersion compared to elastic bars. Zhao and Gary are the first to work on this method, they based their solution on Lundberg ang Henchoz method. They developed an iterative method with frequency domain calculations. Their solution follows this calculation scheme [31] [32]:

$$\begin{cases} \varepsilon_i^{(0)}(x_1, t) = \varepsilon^{(0)}(x_1, t) \\ \left\{ \begin{array}{l} \varepsilon_i^{(k+1)}(x_2, t) = \displaystyle\int_{-\infty}^{+\infty} e^{-i(\xi(\omega)\Delta - \omega t)} \tilde{\varepsilon}_i^{(k)}(x_1, \omega) d\omega \\ \varepsilon_r^{(k+1)}(x_2, t) = \varepsilon^{(k+1)}(x_2, t) - \varepsilon_i^{(k+1)}(x_2, t), k = 0 \dots N \\ \varepsilon_r^{(k+1)}(x_1, t) = \displaystyle\int_{-\infty}^{+\infty} e^{-i(\xi(\omega)\Delta - \omega t)} \tilde{\varepsilon}_r^{(k+1)}(x_2, \omega) d\omega \\ \varepsilon_i^{(k+1)}(x_1, t) = \varepsilon^{(k+1)}(x_1, t) - \varepsilon_r^{(k+1)}(x_1, t) \end{array} \right. \end{cases}$$

Where ε_i is the strain measurement from the incident wave and ε_r is the strain measurement from the reflected wave. x_1 and x_2 are the first and second strain gauge locations and K is an integer bigger than 0.

Using this method Zhao and Gary achieved a test duration of 30 ms which leads to high enough strains for intermediate strain rates. Errors from this iterative method accumulates and increases substantially after 30 ms [32].

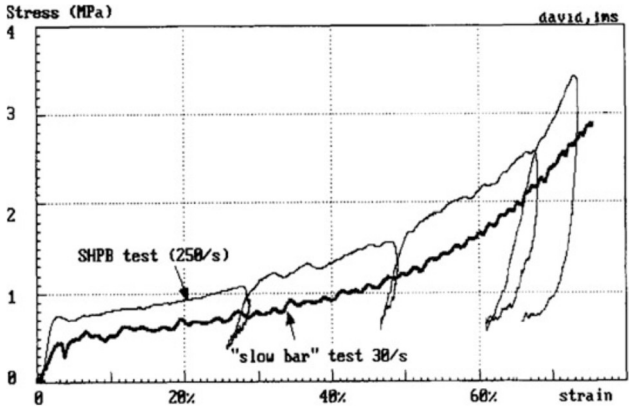

Figure 20: Strain rate effects on foam at medium strain rates [32].

1.3. Numerical Simulations

Numerical simulations are used for design and optimization purposes in many industrial applications. Numerical simulations can be done using implicit or explicit time integration methods. Choice of time integration method depends on the phenomena. Implicit time integration uses bigger time steps however, at each time step, iterations for the solution must be done to achieve a convergence [33]. Generally, this method is used for static applications where there are no nonlinearities in the system. Explicit time integration method uses smaller time steps but does not require iterations. Explicit time integration is used in dynamic problems that have nonlinearities and high deformations. Materials testing under high strain rates require the use of explicit time integration method to achieve accurate and efficient results. Similarly, intermediate strain rate testing also requires explicit time integration methods to capture inertia effects (wave propagation) [33].

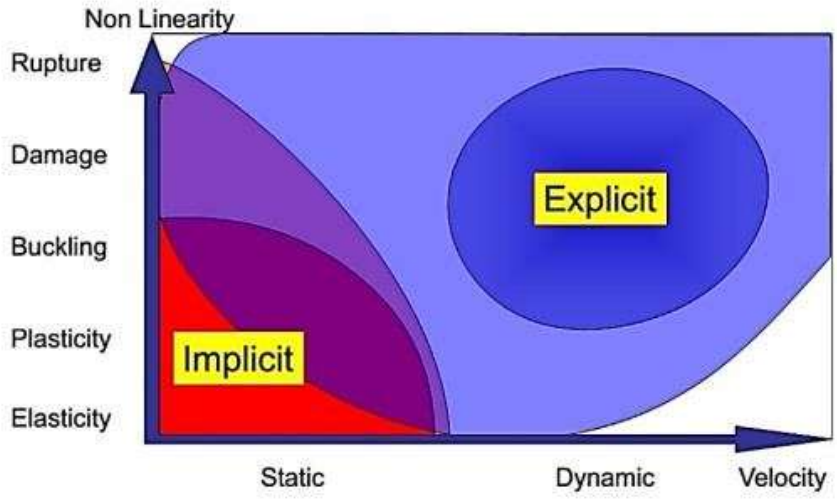

Figure 21: Implicit and Explicit Time Integration Methods [34].

Another important part of finite element analysis is the selection of FEA method selection. There are two important FEA methods used in explicit simulations: Eulerian and Lagrangian methods. Eulerian method is generally used to model fluid or fluid – like materials while Lagrangian method is used for solids. Main difference between the two methods is the movement of the material with respect to nodes. In Lagrangian method nodes are attached to the material while in Eulerian method they are not. Therefore, material follows the node displacements in Lagrangian method. However, in Eulerian method material moves while nodes are fixed. In order to simulate material movement in this method, an advection step is added to FEA chain that fills and empties element volumes with respect to material movement [35].

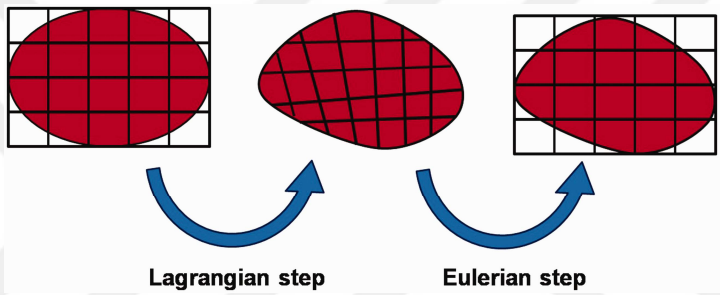

Figure 22: Lagrangian and Eulerian Steps [35].

All finite element simulations in this study were done using LS – Dyna software. LS – Dyna is well – known for its robust explicit finite element solver. It includes many different material models and contact algorithms. It is widely used in automotive and aerospace industry. LS – Dyna was first developed by John O. Hallquist at in 1976. By that time, it was called DYNA3D and was the only 3D simulation software capable of modeling impact. Later on, DYNA3D implemented a general single surface contact for the first time in the world in 1986. In 1988, Livermore Software Technology Corporation (LLNL) was founded and DYNA3D was renamed to LS – DYNA3D. LLNL continuned to develop LS – DYNA in a more focused way with many company collaborations. Finally, in 2019 LSTC was acquired by ANSYS and it still keeps on developing according to industry needs [36].

In this study, a modified Kolsky bar testing system was designed for intermediate strain rate material testing. Numerical simulations in LS – Dyna software was prepared and used for the system's design. After numerical solutions, system was manufactured and tests with three different materials was conducted. Materials chosen for testing was: Polycarbonate, Aluminum alloy 6061-T6 and oxygen free high-conductivity copper. These tests were

repeated to ensure the validity of the results and experimental data was compared to literature and numerical simulations.

Scope of this thesis is the design, production and testing of a novel intermediate strain rate material testing device. Design of the device consists of four main components: loading system, data acquisition, supports and specimens. Each component is selected based on their efficiency and cost. Numerical simulations of the design are performed before assembly to ensure safety. Finally, the system is tested with 3 different materials to prove its validity. Literature data of selected materials are used for comparison and wave separation is applied to reduce noise in test data.

2. NUMERICAL STUDIES

Numerical simulations for the testing system were conducted using LS-Dyna MPP explicit solver. Explicit time integration method was chosen due to dynamic effects and in order to better capture wave propagation in the output bar. Test duration of the system was estimated to be around 20-40 ms, and this duration was used as initial termination value for the analysis. All simulations were done using Intel Xeon E5-2670 CPU with 16 processors and simulation time was approximately 1 hour.

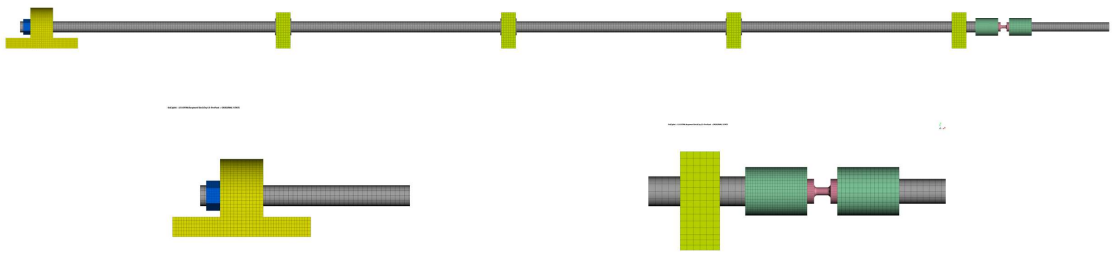

Figure 23: Finite element simulation model of the testing system

2.1. 3D Modelling of the Testing System

Firstly, every part in the testing system was 3D modelled using the Siemens NX, CAD software. Some simplifications were done to these parts to ensure the quality of the mesh and to ensure a high enough timestep size. For example, every threaded part was modelled without threads, small radiuses around the edge of the parts were simplified, bolts are not modelled, loading system was simplified to only its linear rod.

Meshing of the system was done in ANSA pre-processor. This software allows for high quality hexagonal meshing. Resulting meshes can be seen in Figure 24. The finest mesh was used in the specimen since it was the most important part and other parts such as supports was meshed with a coarser grid. Average element size was 5 mm for all parts except the specimen which has a minimum element size of 1 mm.

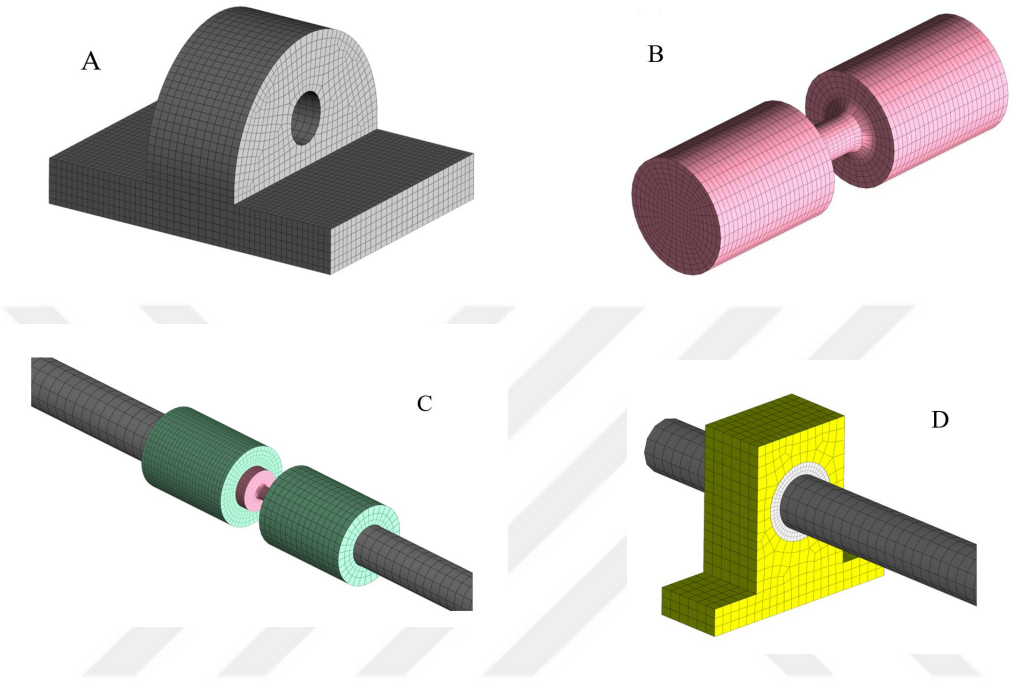

Figure 24: Finite element models of the testing system parts. A: End support, B: Specimen, C: Specimen – Bar interface, D: Linear bearing.

2.2. Simplifications on Boundary Conditions and General Contact

There are many threaded connections used in the testing system. However, modelling threaded parts has a high computational cost. In order to achieve reasonable simulation times and to have a more stable numerical model, tied contacts are used instead of threaded connections. Tied contact assumes that selected regions of the parts move together and are inseparable unless there is erosion in one of the parts. Since, all parts in the testing system remains elastic during tests, no erosion will occur and tied contacts can model threaded connections good enough.

Furthermore, testing system was fixed to the ground by long bolts in the concrete. In numerical simulations, system is fixed using simple boundary conditions. This is an artificial constraining method and does not allow any movement or rotations at the selected nodes.

This is also a good enough approach because no movement is expected at the ground supports and they are always elastic. These boundary conditions and part connections are shown in Figure 25.

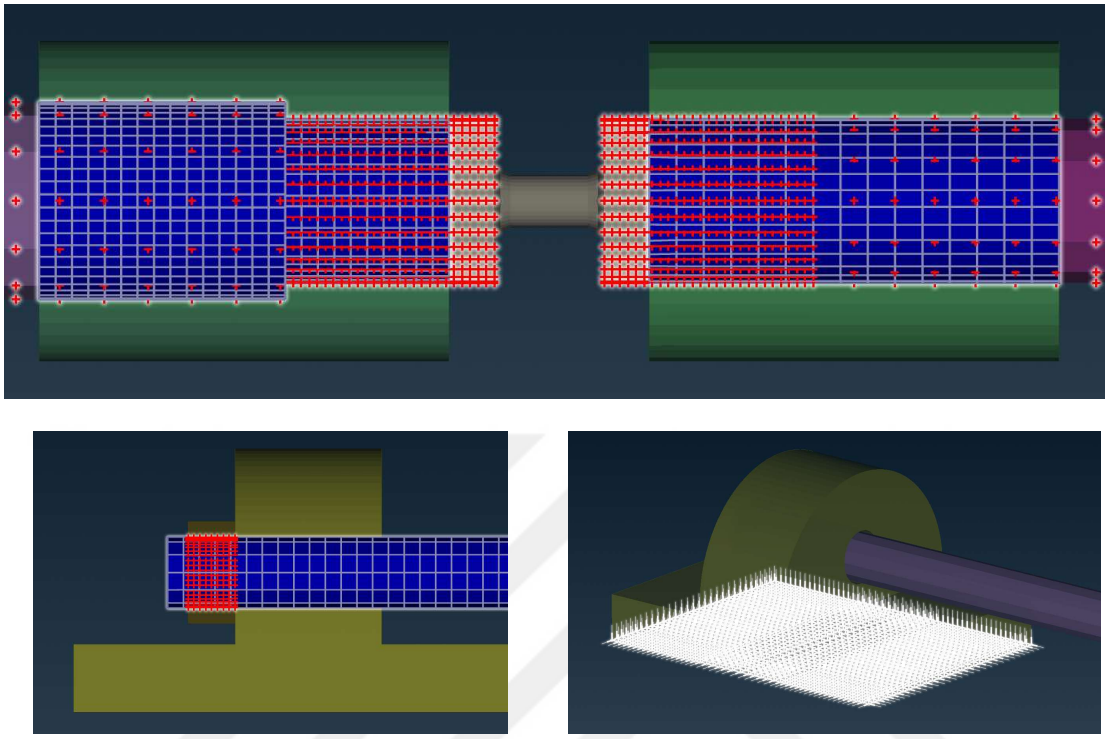

Figure 25: Tied contact and fixed boundary conditions applied to parts with threaded and bolted connection.

General contact in the numerical simulation is handled by CONTACT_AUTOMATIC_SINGLE_SURFACE keyword. This keyword allows for a simple and robust penalty contact algorithm to be applied to every surface of every part. This keyword has many parameters and most of them were left as default. These parameters can be seen below in Table 1.

Table 1: Contact keyword parameters

***CONTACT_AUTOMATIC_SINGLE_SURFACE**				
FS	FD	DC	VC	VDC
0.80	*0.40*	*10.0*	*5.0e+8*	*10.0*
SOFT	SOFTSCL	MAXPAR	SBOPT	DEPTH
2	*0.10*	*1.025*	*2.0*	*2*

2.3. Material Models

There are two material model keywords. used in this study: MAT_ELASTIC and MAT_SIMPLIFIED_JOHNSON_COOK.

MAT_ELASTIC is a material model that is used for materials that are perfectly elastic. For this keyword only Elastic Modulus, density and the Poisson ratio of the material is required as inputs. All parameters for the material model and parts that it is used on is given in Table 2.

Table 2: Material model parameters for MAT_ELASTIC

***MAT_ELASTIC (4340 Steel) [4]**				
RO	E	PR	DA	DB
7830	*2.10E+11*	*0.30*	*0.0*	*0.0*

MAT_SIMPLIFIED_JOHNSON_COOK keyword is a simplified version of the commonly used Johnson – Cook material model. Johnson – Cook material model consists of a strain hardening, strain rate hardening and temperature softening strength model and a triaxiality based damage model with two additional parameters for strain rate and temperature effects on failure strain. In this study, only the strength of a material under intermediate strain rates are of interest. Therefore, a detailed failure model is not required. Furthermore, no significant adiabatic heating is expected for the specimen which means temperature effects can be neglected as well.

Simplified Johnson – Cook model neglects temperature effects and does not have a failure model. Instead, it uses a maximum stress parameter to account for the temperature softening and a simple maximum failure strain parameter for failure. This model is much less expensive than Johnson – Cook model and is adequate for this study. Therefore, it was chosen to be used for the specimen material. Three materials (Polycarbonate, Aluminum and Copper) were modelled with Simplified Johnson – Cook. Parameters for materials was taken from literature except for copper for which custom parameters determined by TUBITAK SAGE is used and these parameters are given in Table 3.

Table 3: Material model parameters for Simplified Johnson - Cook Material Model

***MAT_SIMPLIFIED_JOHNSON_COOK**

Steel 4340 [4]				
RO	E	PR	VP	
7830	*2.10E+11*	*0.30*	*0.0*	
A	B	N	C	PSFAIL
7.92E+8	*5.10E+8*	*0.26*	*0.014*	*0.2*
Polycarbonate [37]				
RO	E	PR	VP	
1190	*2.54E+9*	*0.344*	*0.0*	
A	B	N	C	PSFAIL
7.6E+7	*6.9E+7*	*1.00*	*0.0*	*1.20*
OFHC Copper				
RO	E	PR	VP	
8960	*1.10E+11*	*0.34*	*0.0*	
A	B	N	C	PSFAIL
3.13E+8	*3.53E+8*	*1.1615*	*0.1616*	
Aluminum 6061-T6 [4]				
RO	E	PR	VP	
2700	*6.9E+10*	*0.33*	*0.0*	
A	B	N	C	PSFAIL
3.24E+8	*1.14E+8*	*0.42*	*0.002*	

2.4. Data Collection

Data collection from numerical simulations were done similarly to the real test since, the results of the numerical simulations will be compared to the real test results. Three strain gauge locations were selected and DATABASE_HISTORY_ELEMENT keyword was used to record element output at these locations during the simulations. From these outputs strains at these locations are gathered similar to real strain gauge data. Locations of these gauge points can be seen in Figure 26.

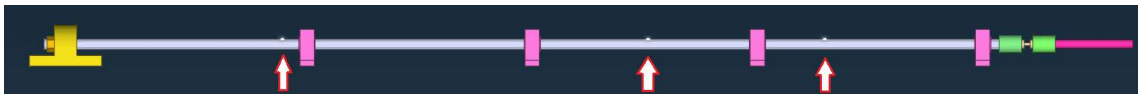

Figure 26: Strain gauge locations for the finite element model.

3. EXPERIMENTAL STUDIES

3.1. Design of the Intermediate Testing System

The aim of this study is the design and application of an intermediate strain rate material testing system that is capable of extracting data of materials under intermediate strain rates with high repeatability and low noise. To achieve this aim, testing device must have these qualifications:

- Testing system must be able to reach at least 10^1 s^{-1} strain rate and must be able to test lower strain rates. Generally accepted range for intermediate strain rate is between 10^0 s^{-1} and 10^2 s^{-1}.
- Testing system must have high duration of loading to achieve failure of the material. This depends on the material tested but for 10^1 s^{-1} strain rate and 25% failure strain, this duration is equal to $t = \frac{0.25}{10} = 0.025$ s.
- Testing system must be able to withstand high strength materials.
- Testing system must have high repeatability and low noise due to inertia effects.

Considering the requirements, above only servo – hydraulic and similar linear actuator loading systems can achieve high test durations and high loads. Other alternatives such as drop towers and long Kolsky bars have shortcomings if these requirements are considered. For example, drop tower test systems cannot test lower end of the intermediate strain rates and have high noise due to inertia effects. Long Kolsky bars can achieve most of the required properties except for 10^0 s^{-1} strain rates. However, they require very large working places because the transmission bar needs to be 10+ meters long.

Intermediate strain rate testing system generally suffer noise due to inertia effects which is due to wave propagation. This effect is more visible in 10^2 s^{-1} strain rates. Commercial load cells cannot measure reliable data under these conditions. Therefore, a Kolsky bar load measurement system is chosen for this testing system. A transmission bar directly threaded to the specimen with strain gauges cemented at different locations on the bar is used. This transmission bar needs to be fixed on the other end to ensure high testing durations.

For strain measurements, high – speed cameras can be used. Kolsky method for strain measurement cannot be used since the specimen needs to be connected to the loading system and Kolsky method requires an incident bar with strain gauges. There are many open – source codes that allow for digital image correlation using high – speed camera results.

3.1.1. Loading System

Loading system of the testing system is chosen to be a servo electromechanical actuator which can achieve high speed and withstand high loads. This type of actuators is commonly used in universal testing systems. However, their exact parameters such as speed, acceleration, maximum load and stroke length must be customized for the application.

Servo – electromechanical actuators use brushless servo motors coupled with power screws to achieve controlled movement of the desired type. Speed, acceleration and the force of the movement depends on the capabilities of the servo motor and the power screw it is coupled to.

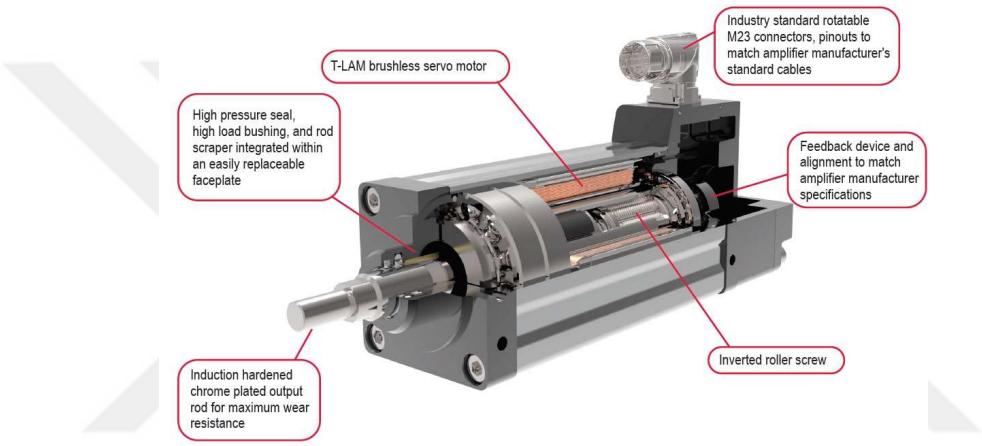

Figure 27: Example of a servo electromechanical linear actuator [38].

In this study, a servo electromechanical linear actuator was used without a reductor which would increase the force but reduce speed. Instead, servo motor was directly coupled to linear actuator. In this way, higher speed and acceleration was achieved. Siemens 1FL6094 servo motor was used in this study. Specifications for this servo motor is given in Table 4.

Table 4: Specifications of Servo Motor

Siemens 1FL6094-1AC61-2LB1

Motor Type	High Inertia Permanent-Magnet Synchronous Motor
Rated Speed	2000 rpm
Maximum Speed	2500 rpm
Rated Torque	23.90 Nm
Maximum Torque	70.00 Nm
Rated Power	5.00 kW / 6.80 hp

Figure 28: Siemens 1FL6094 Servo Motor

Together with the linear actuator mechanism in Figure 27 this loading system is capable of the following loading conditions:

- 350 mm/s maximum linear speed.
- 7 m/s^2 maximum acceleration.
- 8 kN maximum allowable load.

Using these properties strain rate that will be achieved for a standard round specimen with a gauge length of 14 mm is calculated as follows:

$$\dot{\varepsilon} = \frac{v}{l} = \frac{0.350}{0.014} = 25\ s^{-1} \tag{19}$$

Where v is the actuator speed, l is the specimen length and $\dot{\varepsilon}$ is the strain rate. The maximum stress allowed for the specimen with a 6 mm diameter is also calculated as follows:

$$\sigma = \frac{F}{A} = \frac{8000}{0.003^2 \cdot \pi} = 283\ \text{MPa} \tag{20}$$

Where F is the maximum allowed load for the loading system and A is the gauge area. According to this calculation the loading system should have no problem testing a material under 25 s^{-1} and up to 283 MPa maximum stress. Higher stress values can be achieved at the cost of a lower lifetime for the linear actuator or by reducing the diameter of the specimen.

3.1.2. Data Acquisition

There are two crucial output data that is required to interpret behavior of the materials: stress and strain. In this study, high – speed camera is used to record strain of the material during testing and strain gauges applied to an output bar is used to record material stress.

SA – Z model high – speed camera is used with 25,000 fps and two spotlights focused on the specimen. High speed camera setup is given in Figure 29.

Figure 29: High Speed Camera

Three strain gauges were applied to the output bar coupled to the specimen. These strain gauges record the strain of the output bar during the test. Output bar is made out of AISI 4340 steel which is completely elastic during testing. This was ensured before testing by finite element analysis. Three strain gauges are used in order to use the wave separation method of Jacquelin and Hamelin to reduce noise in strain data. Strain gauges were connected to Dewesoft data acquisition system during tests and strain data was recorded with the help of the Dewesoft software. Connections of the three strain gauges and the data acquisition system can be seen in Figure 30.

Figure 30: Strain gauges and Dewesoft data acquisition system

3.1.3. Supports and Moving Parts

Testing system consists of a linear actuator coupled to the specimen by a threaded connector which is also attached to the output bar on the other side of the specimen. Output bar is fixed at two meters away from specimen/bar interface by a fixed support and output bar is supported by linear bearings in the middle. All parts are attached to an I beam by bolts and nuts. I beam is attached to the ground by twelve long bolts and three locations.

Fixed end support is required to fix the free end of the output bar. Without the fixed support specimen would move together with the linear actuator and only small strains would be seen in the specimen. Fixed end support is made out of 4140 steel to ensure it always stays elastic during testing and it is bolted to the I beam at four different locations by M27 bolts. Output bar is threaded at its end so that it can be attached to the fixed end support with a nut. This nut is M24 and it also needs to be elastic during testing. It is expected that this nut will hold the most severe stress during testing therefore, numerical simulations are done to ensure it is elastic during testing. Fixed end support and how it is attached is shown in Figure 31.

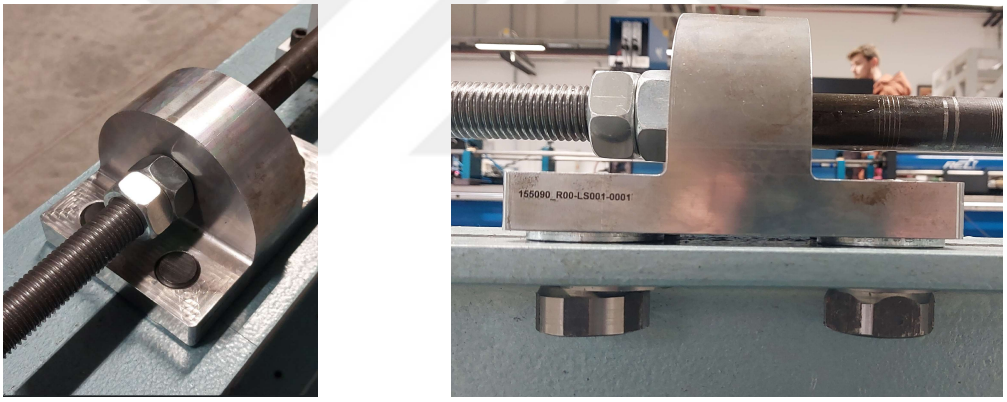

Figure 31: Fixed end support part.

There are three linear bearings used to support the output bar and keep it as straight as possible along its length. These linear bearings only carry the weight of the bar and does not need to be high strength. However, output bar must pass along the linear bearings with ease and friction should be minimum. In order to ensure this, polymer inserts made out of PTFE material is used and lubricant is applied between the output bar and linear bearings. Linear bearings are shown in Figure 32.

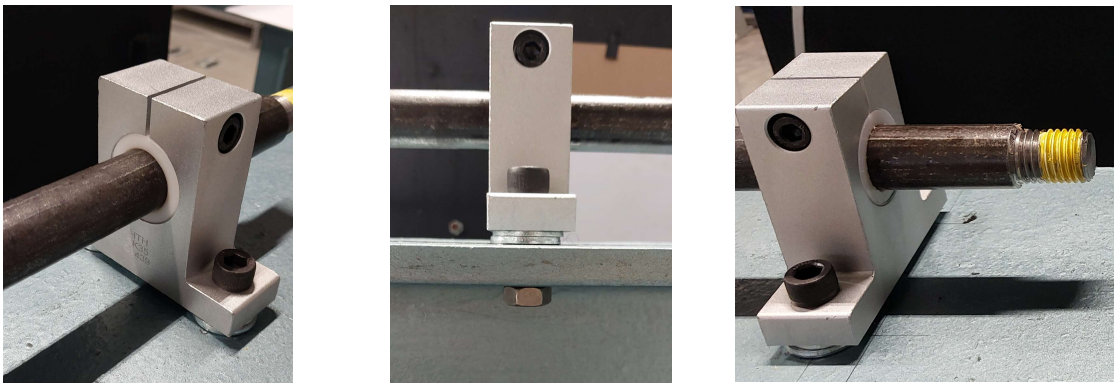

Figure 32: Linear bearings

For this testing system, 2 meters long 4340 steel output bar is used. This bar has a diameter of 24 mm and is threaded at both its ends for the necessary connections. This bar is used to measure the stress of the specimen during the test via strain gauge recordings. Therefore, the bar must stay elastic during the testing in order to ensure stress calculations from strain gauge data is correct. To ensure this, numerical simulations are conducted and it was seen that the diameter of the bar is sufficient and it is elastic at all cross sections.

Testing system is put on an I beam with IPE 300 standard. This I beam is chosen because it was easy to obtain and it has good strength properties. I beam is attached to three steel plates. These steel plates are used to fix the testing system to the ground. This is achieved by bolting the steel plates to the concrete ground by bolts and fixing the I beam to the steel plates by bolts and nuts. This connection and I beam can be seen in Figure 33.

Figure 33: I beam and ground connections.

Finally, specimen needs to be attached to both the loading system and the output bar. Threaded connection is chosen for this and two specimen interface parts are produced. These parts have two different threaded regions which are used to attach the specimen on one side and the loading system and output bar on the other side. These interface parts are made out of the same material as the output bar which was 4340 steel to ensure a correct impedance match. These connection parts can be seen in Figure 34.

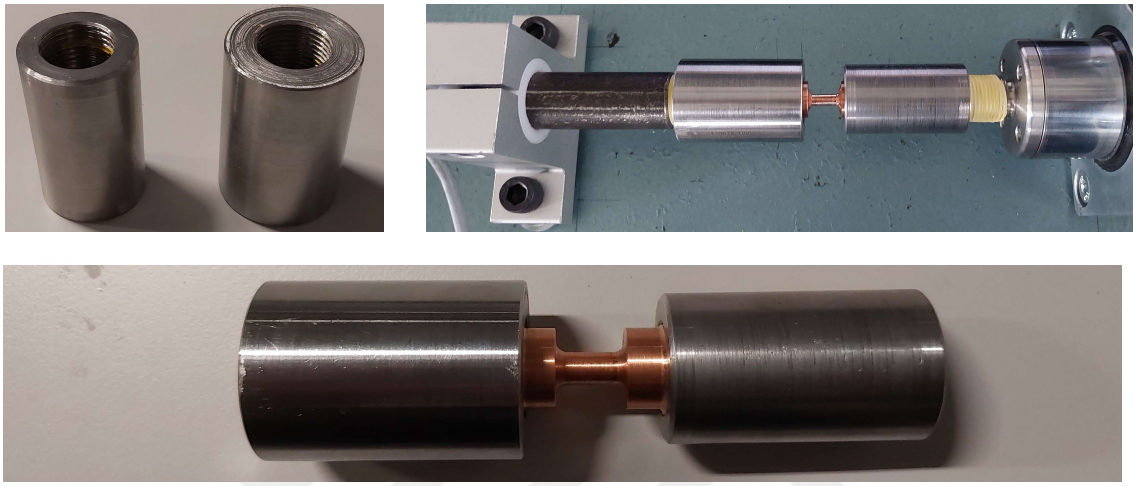

Figure 34: Specimen interface parts.

3.1.4. Specimens

In this study, only uniaxial tension tests are conducted and therefore, only one type of specimen is used. This specimen had a diameter of 6 mm and a gauge length of 13.5 m which results in a L/D ratio of approximately 2. The diameter of the specimen is modified to meet the maximum load requirement set by the linear actuator and the length of the gauge length is chosen according to the strain rate goal. A longer specimen gauge length would result in a lower strain rate and vice versa. Specimens are machined at both ends with threads required to attach them to the testing system. In this study, 3 different type of material was examined: Polycarbonate, aluminum 6061 – T6 and OFHC copper. Specimen pictures are shown in Figure 35.

Figure 35: OFHC Copper, AA6061-T6 and Polycarbonate specimens.

3.2. Assembly of the Testing System

The final state of the testing system is given in Figure 36. Linear actuator is controlled by a laptop and strain gauges are connected to the data acquisition system. High – speed camera can record up to 2 seconds, so it can be easily triggered manually and no automatic triggering was used. Specimen is connected to the system via threads on interface parts and the output bar is fixed at its end.

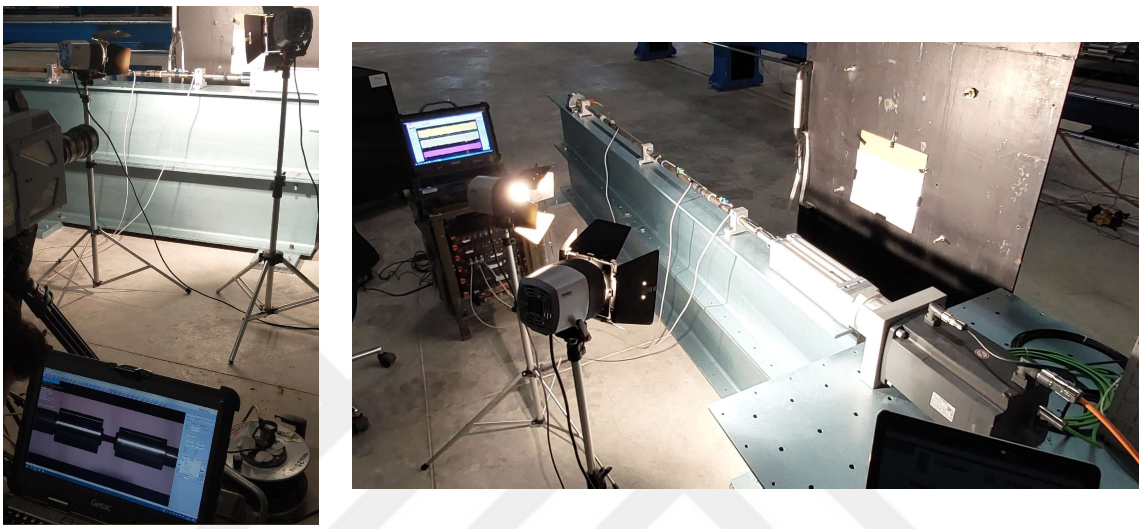

Figure 36: Assembly of the testing system.

3.3. Conducted Tests

Total of 4 test are conducted with 3 material types. These are given in Table 5.

Firstly, a trial test was conducted without a specimen to measure the sound speed of the output bar. This information is used in wave separation calculations and to find out the Elastic Modulus of the output bar. Sound speed is calculated by the time difference of the stress wave arrival between the strain gauges on the output bar. Afterwards, 4 tests with 1 Polycarbonate, 1 AA6061-T6 and 2 OFHC Copper specimens was conducted. Results of these tests are given and discussed in the next section.

Table 5: Conducted experiments and materials

Test No	Material
1	For sound speed calculations
2	Polycarbonate
3	AA6061-T6
4	OFHC Copper
5	OFHC Copper

4. RESULTS AND DISCUSSIONS

4.1. Numerical Results

Main purpose of numerical simulations for this study was ensuring the material strength results obtained from experiments are similar to material response in simulations. Materials used in experiments are commonly used engineering materials, therefore there are many sources for material model parameters. Loading and failure of the specimen can be modeled and this is shown in Figure 37.

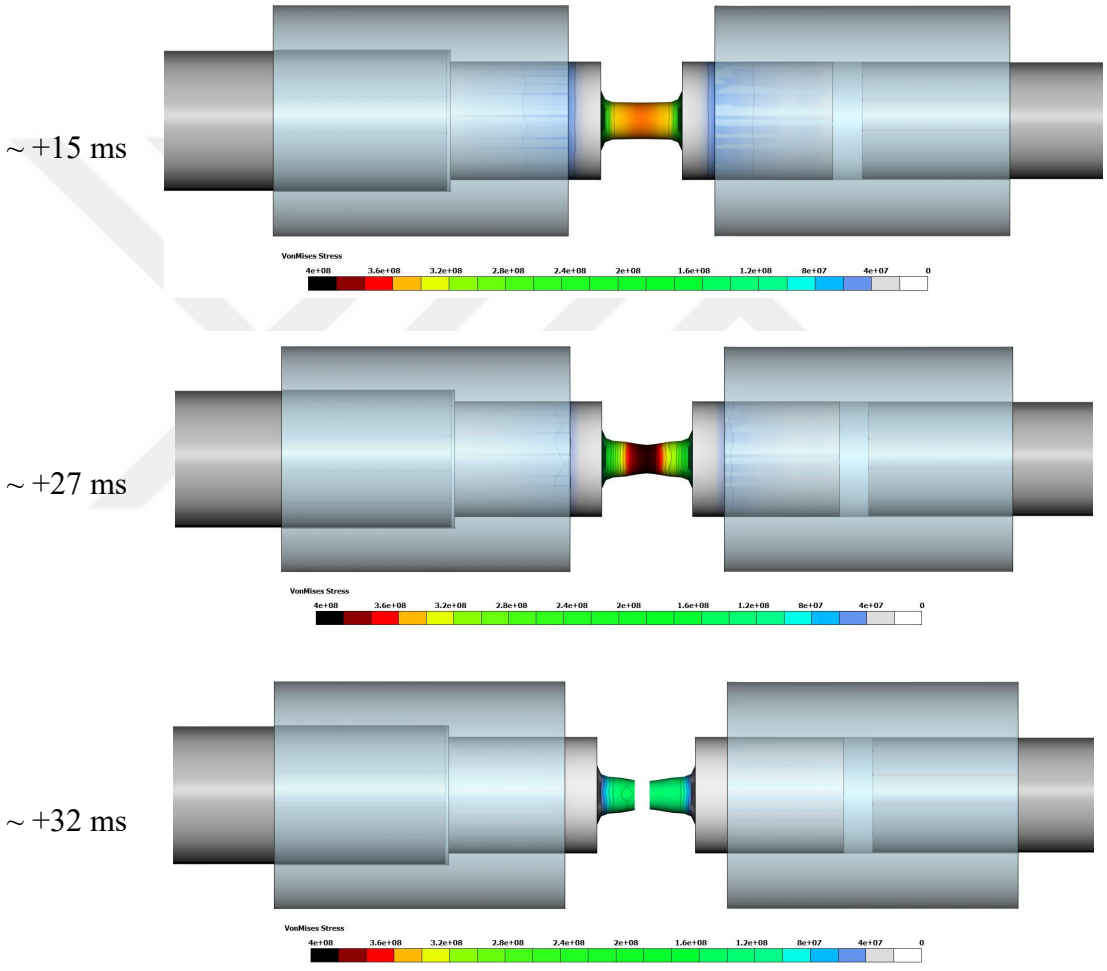

Figure 37: Finite element simulation showing failure of a specimen

Numerical simulations were done for all materials and results obtained from the strain gauges are plotted in Figure 38.

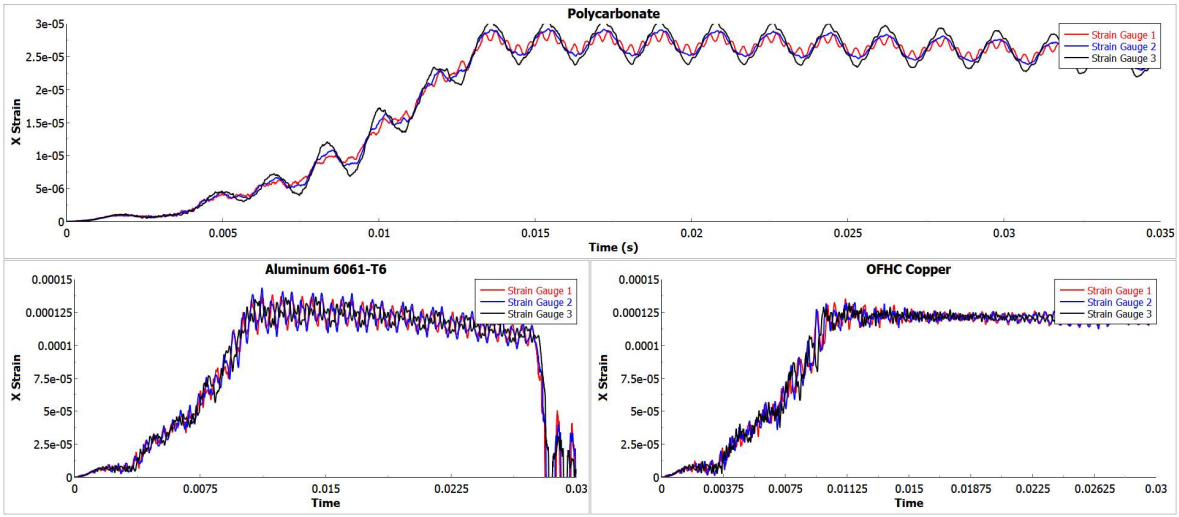

Figure 38: Strain data obtained from numerical simulations

From Figure 38 it can be seen that there is an oscillation in the strain data as expected due to wave propagation in the output bar. However, the strain data is adequate enough to determine material response, especially if only strain gauge 1 data is considered. Even though strain gauge 1 data is good enough for material response prediction, wave separation is applied to the simulation results to reduce noise. For wave separation, method of Jacquelin and Hamelin [28] was used and results are shown in Figure 39.

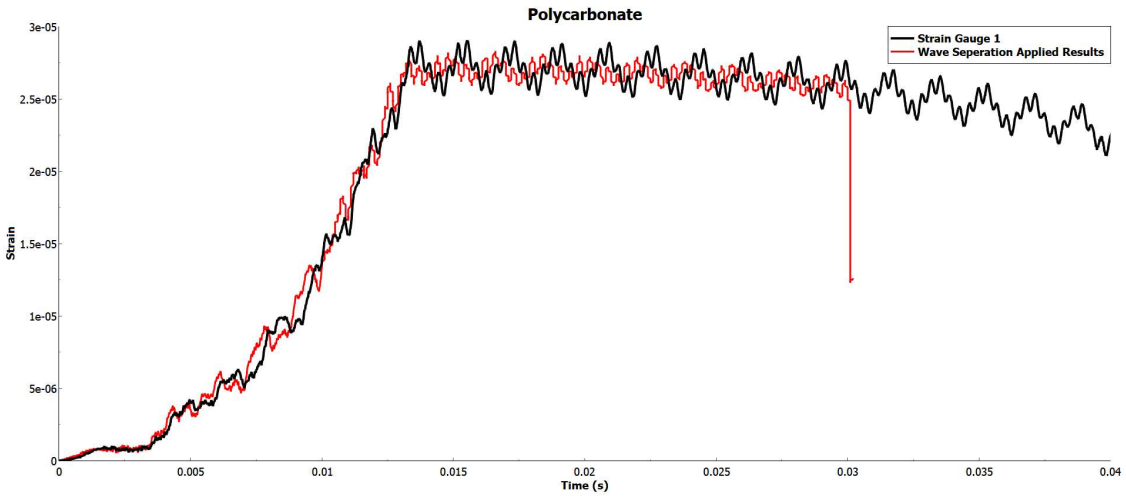

Figure 39: Wave separation applied to strain gauge data from numerical results.

Examining Figure 39 it can be seen that wave separation method reduces noise but it does not make a significant difference to results. This method may be more effective for strain rates higher than 50 s^{-1}, because wave propagation effect increases with increasing strain rate. Finally, (6 is used with the strain data from numerical simulations to obtain specimen stress. Results are shown in Figure 40.

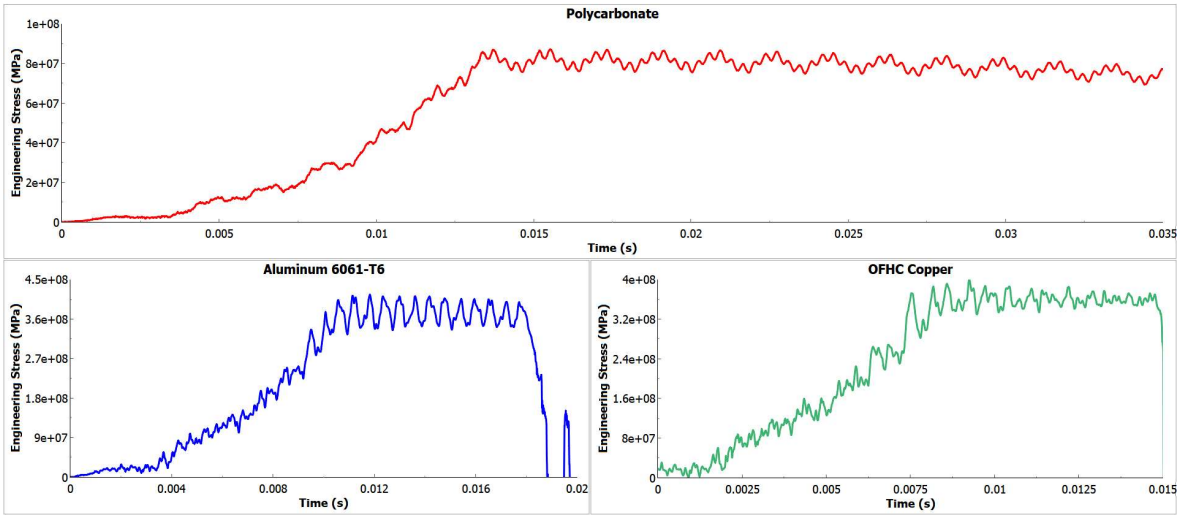

Figure 40: Engineering stress vs. time results of Polycarbonate, AA6061 - T6 and OFHC Copper materials.

4.2. Experimental Results

First experiment conducted in this study was without a specimen in order to measure the sound speed of the output bar which is a necessary input for wave separation calculations. Output bar was struck with a hammer and strain gauge data was collected. Strain gauge results of this test is given in Figure 41.

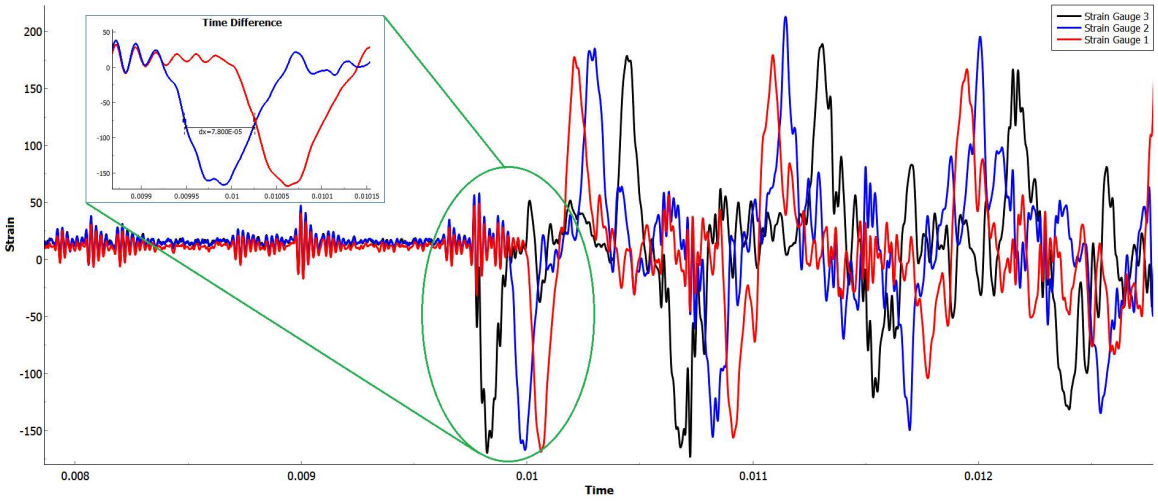

Figure 41: Strain gauge results for test 1.

Distance between the strain gauges are known and using the data from Figure 41, sound speed of the output bar material is calculated as follows:

$$v = \frac{Dx}{Dt} = \frac{0.405}{(7.8) \cdot 10^{-5}} = 5192 \frac{m}{s} \quad (21)$$

Next, using the sound speed of the material, elastic modulus is calculated. Density of the material ρ is taken from literature [3].

$$E = v^2\rho = (5192)^2(7830) = 211\ \text{GPa} \tag{22}$$

After the sound speed experiment, 8 tests are conducted with 3 different materials. First material tested was Polycarbonate. Specimen attached to the testing system can be seen in Figure 42.

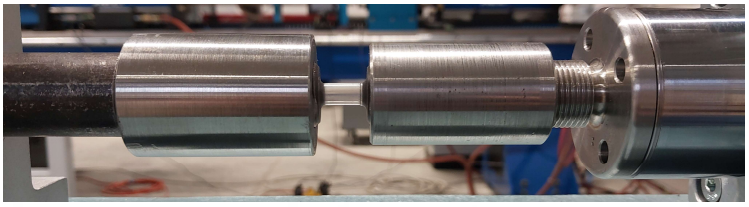

Figure 42: Polycarbonate specimen connected to the testing system.

For this test, High speed camera images are given in Figure 43, and strain gauge data is given in Figure 44.

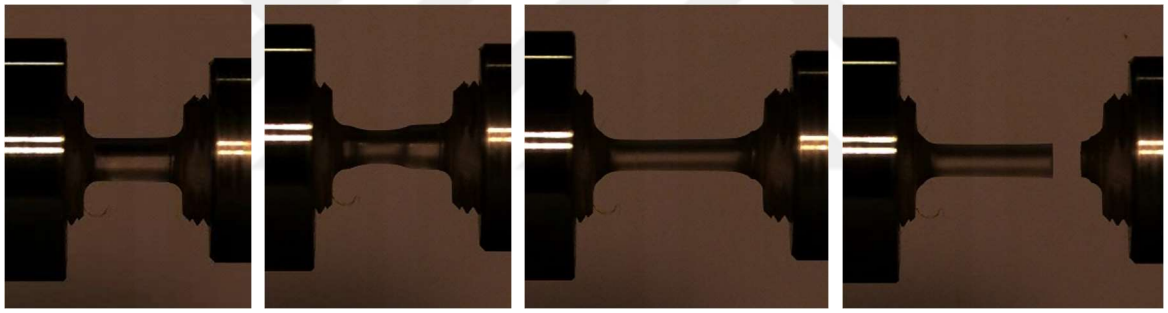

t = 0 t = ~30 ms t = ~50 ms t = ~60 ms

Figure 43: Polycarbonate experiment high speed camera images

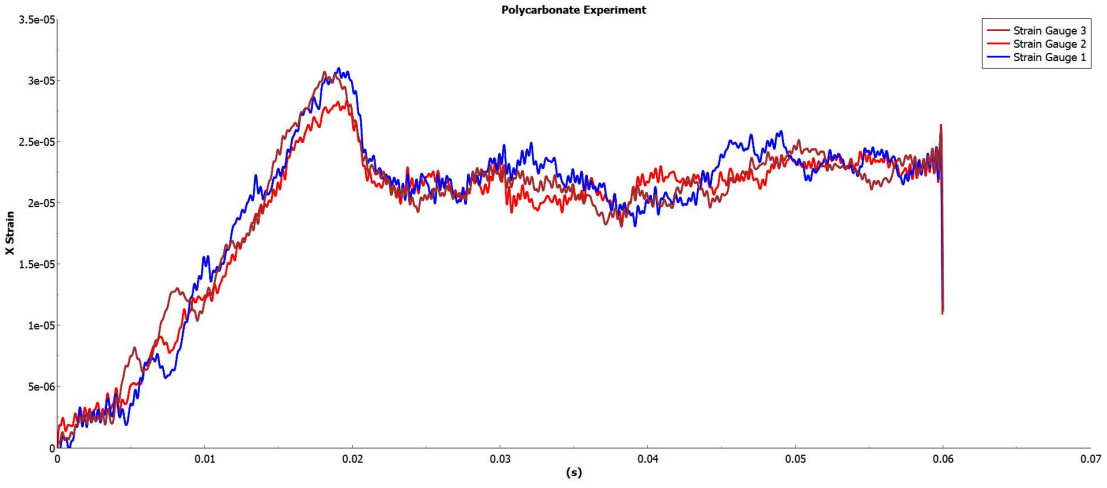

Figure 44: Strain gauge data from Polycarbonate experiment.

Polycarbonate showed highly ductile behavior in this experiment. From the high-speed camera images from Figure 43, it is seen that necking occurs after yield and material continues elongating until fracture. All strain gauge data was filtered using a 4 kHz low pass filter to reduce experimental noise. All strain gauge results were similar as expected which suggests a good alignment of the specimen. Wave separation applied to the strain gauge data is given below Figure 45.

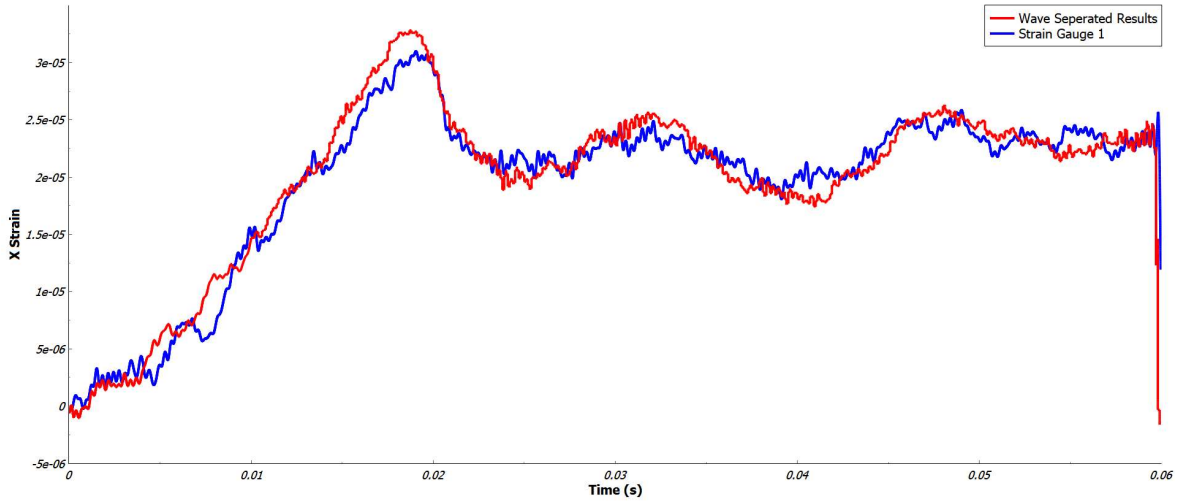

Figure 45: Wave separation applied to polycarbonate test data.

Using wave separation applied strain gauge data, engineering stress of the specimen during testing is calculated. This is shown in Figure 46. Maximum stress seen was approximately 95 MPa for this test and test duration was 60 ms.

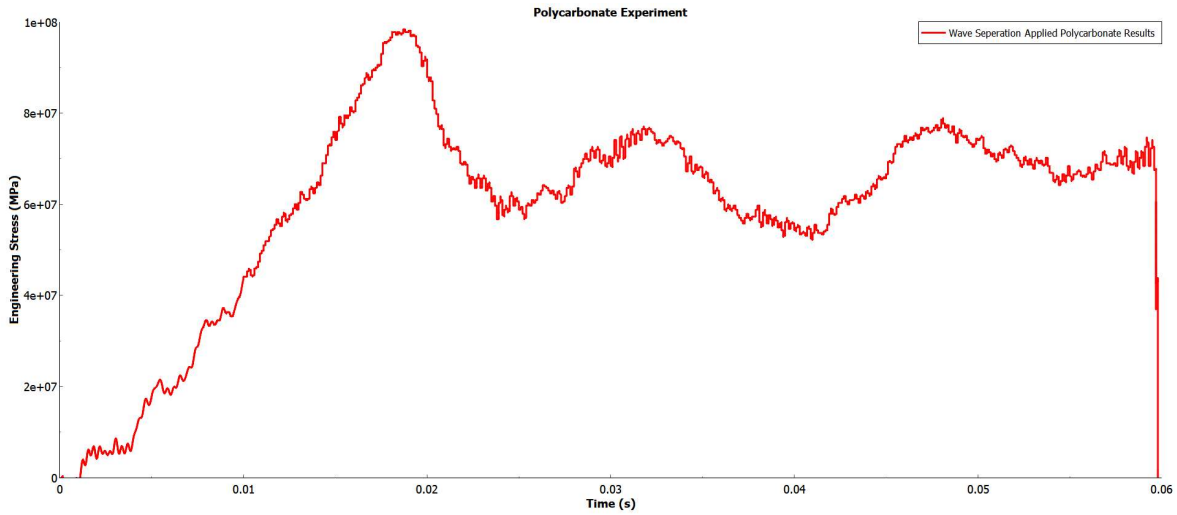

Figure 46: Engineering stress vs. time plot of Polycarbonate experiment.

In order to calculate the strain of the material high speed camera images were processed using an open-source image correlation software. Results of the image correlation can be seen in Figure 47 which shows strain and strain rate observed in this experiment.

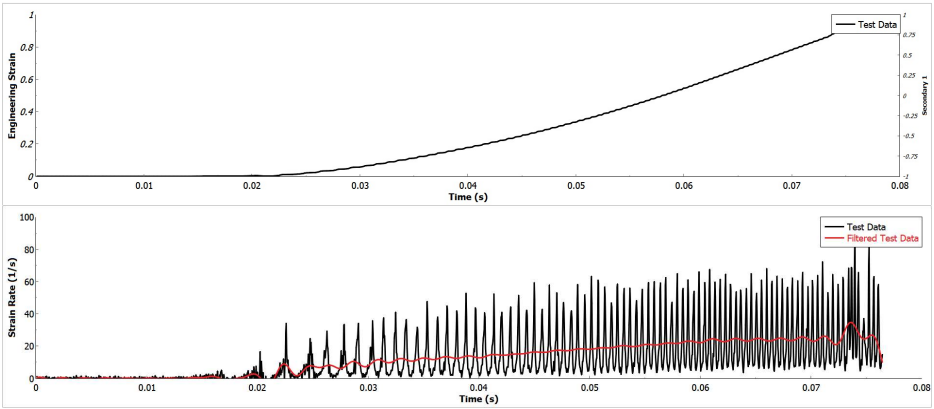

Figure 47: Strain and strain rate results from Polycarbonate experiment.

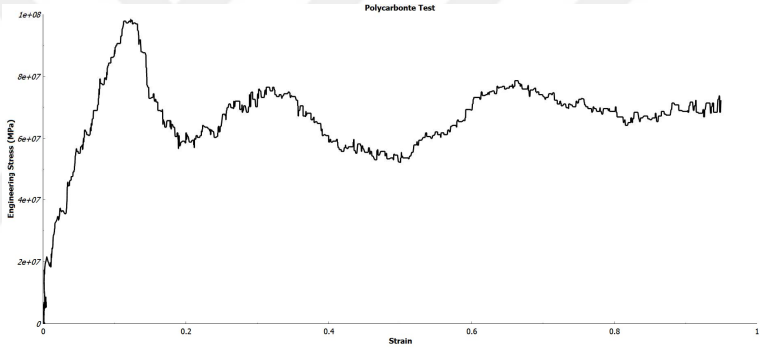

Figure 48: Engineering stress vs. engineering strain plot for Polycarbonate.

From these results it is seen that a strain rate of approximately ~20 s^{-1}, a maximum engineering strain of almost 1 and maximum stress of 95 MPa is achieved with this testing system. Strain rate data has high noise, this is thought to be due to the resolution of the high-speed camera image which affects image correlation accuracy. Strain rate is within the intermediate strain rate range and maximum strain achieved is very high, these test results show that the intermediate strain rate testing system works as intended for highly ductile Polycarbonate material.

Other than Polycarbonate two more materials were tested. These were OFHC copper and Aluminum alloy 6061-T6. Both materials are widely used in many engineering applications. Similar to Polycarbonate, strain gauge data and high-speed camera images were collected and processed to obtain engineering strain vs. engineering stress curves as well as strain rate data.

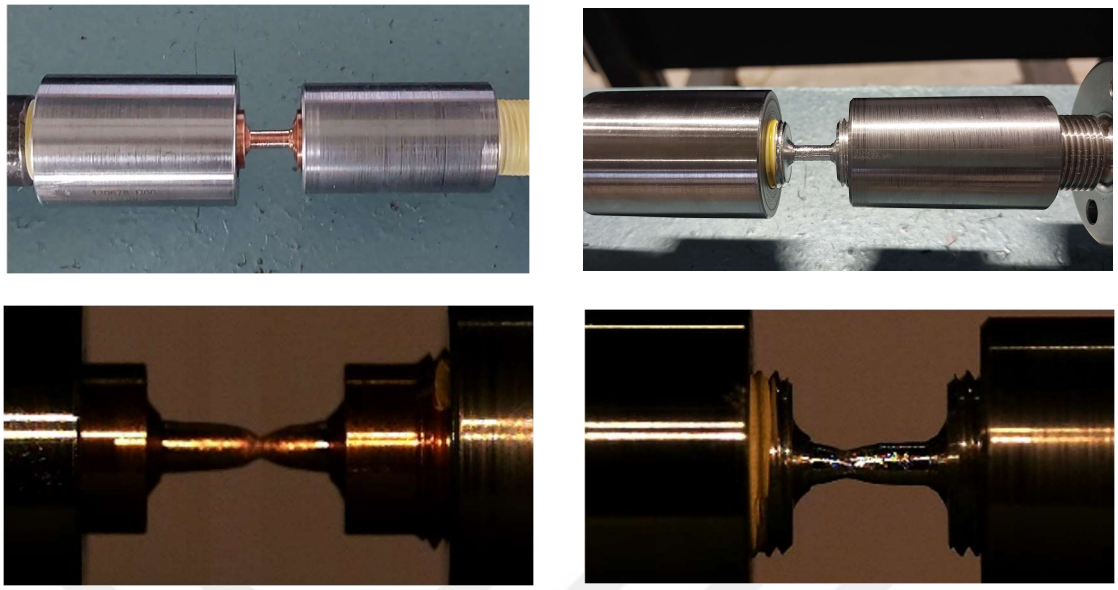

Figure 49: OFHC Copper and Aluminum 6061 T-6 Specimens before testing and before fracture.

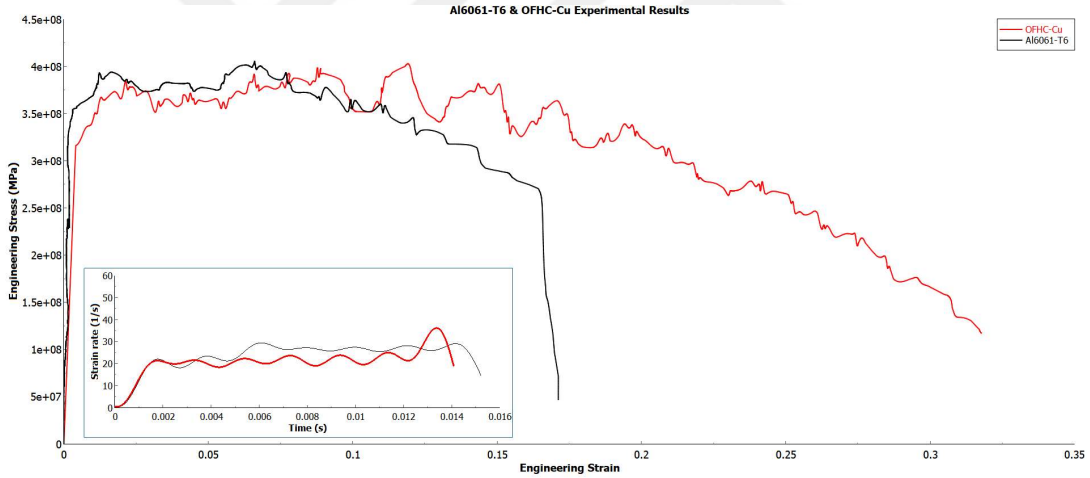

Figure 50: Experimental results of OFHC Copper and Aluminum 6061-T6 materials.

In both AA6061-T6 and OFHC Copper materials, noise levels were lower compared to Polycarbonate even though strain rates were similar. Maximum elongation observed for the copper material was approximately 32% and for aluminum it was 16%. However, these measurements do not factor in the necking region where non uniform stress state is dominant. When the high camera images are examined (Figure 49), it can be seen that copper and aluminum fracture strain is higher. Yield stress of copper was measured as approximately 350 MPa and aluminum 400 MPa. In both test results intermediate strain rate is achieved with an almost constant strain rate value of 20 s^{-1}.

Finally, OFHC – Copper test is repeated to investigate repeatability of the testing system. Same type of specimen was tested with exactly the same conditions for this purpose. Results of these tests are given below in Figure 51.

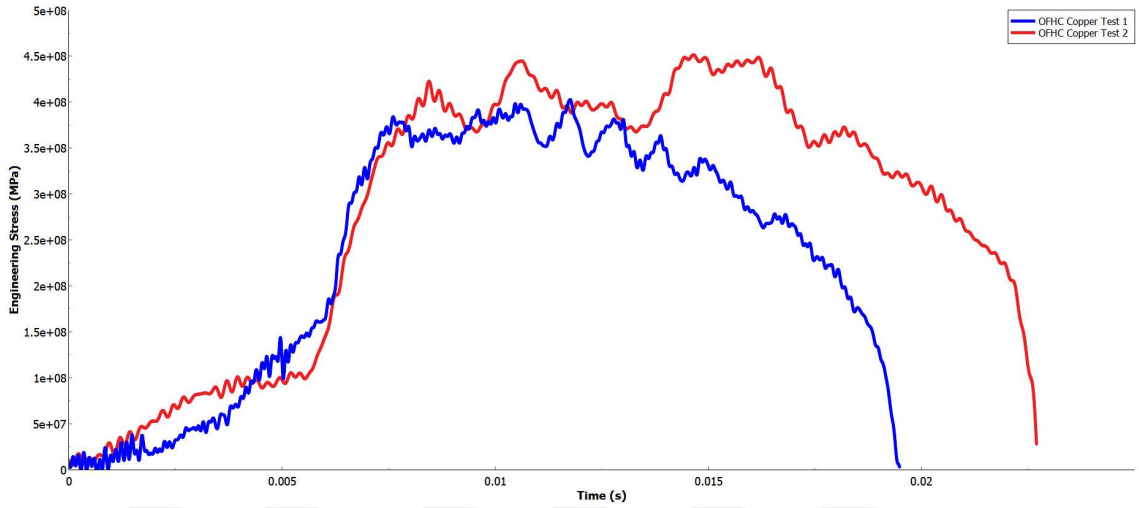

Figure 51: Comparison of two OFHC Copper tests.

Comparing these two tests in Figure 51, it can be seen that both test results are very similar until yield occurs. After this point, results start to diverge from each other. This is thought to be because of necking behavior and surface finish of the specimens.

4.3. Discussions

Aim of this study was to design and produce an intermediate strain rate testing device and show its application. In the previous sections, test results and numerical simulations used in the design of this system is given. In this section, a comparison of numerical simulation results and experimental results will be presented. Furthermore, experimental results will be compared to literature data.

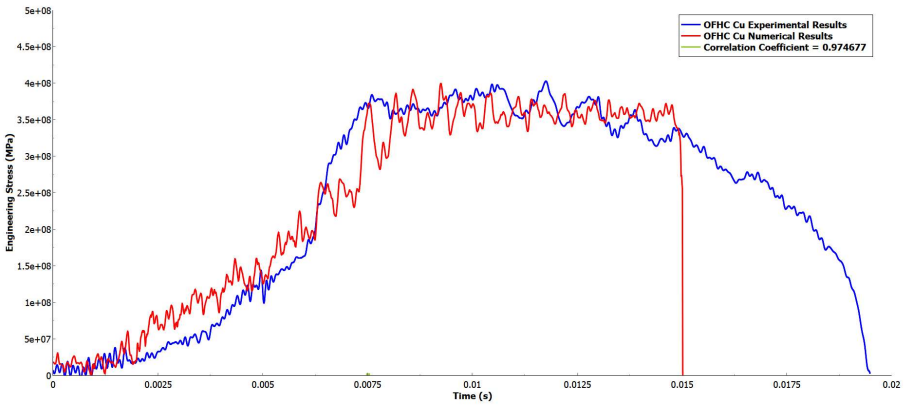

Figure 52: OFHC Copper experimental and numerical results comparison.

Numerical and experimental results are compared in Figure 52 for OFHC Copper material. A very good match of experimental and numerical results is observed and a correlation coefficient of 0.976 is obtained.

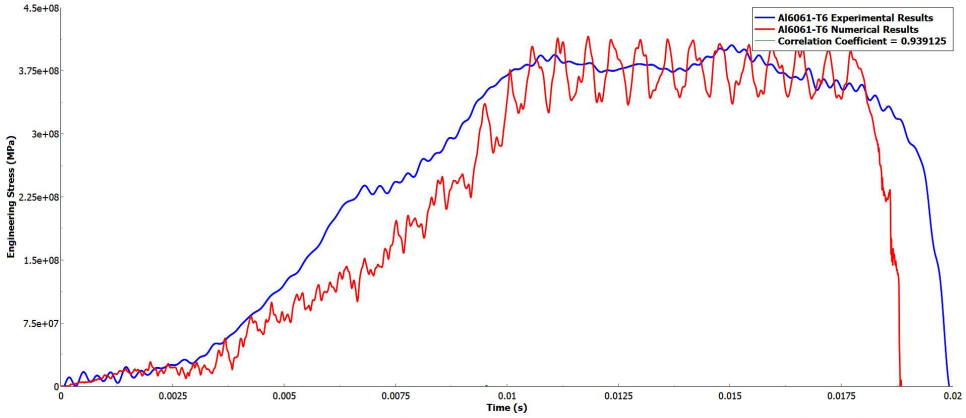

Figure 53: AA6061-T6 experimental and numerical results comparison.

In Figure 53, AA6061 – T6 material experimental and numerical simulation results are compared. Good match of experimental and numerical results is observed and a correlation coefficient of 0.939 was obtained. This is lower than Copper material but it is still considered a good match, especially post yield region fits well with numerical data. There is some error during the elastic flow of the material. This can be due to threaded connections and how they are represented in the finite element model. Finite element model constraints movement at the connections, however in reality there is a small movement at first which affects the results.

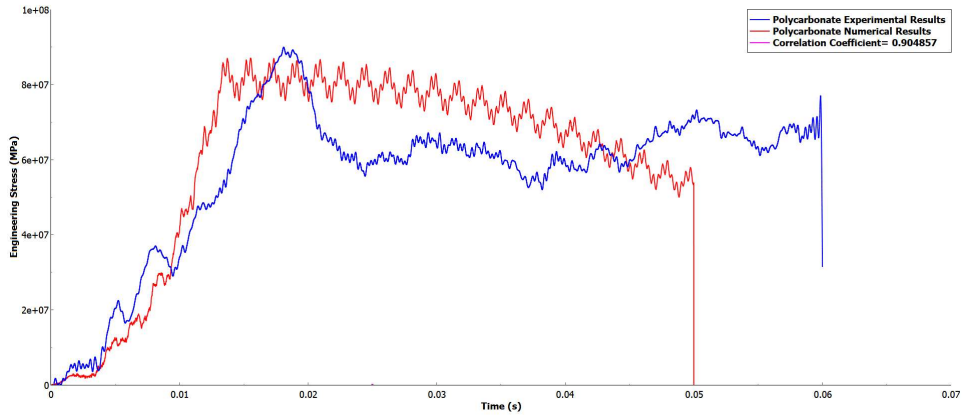

Figure 54: Polycarbonate experimental and numerical results comparison.

Figure 54 shows the correlation of numerical and experimental results for Polycarbonate material. Correlation coefficient for this comparison was 0.905, which was lower than other materials but it is still considered to be an adequate match. The most significant different between numerical and experimental results for Polycarbonate resulted from its post yield flow. Johnson – Cook material model used for Polycarbonate material in the finite element model is widely used for metallic materials and cannot represent polymers as well as metals. Necking and the expansion of the necking region plays an important role in Polycarbonate material's strength and these instabilities cannot be represented in finite element model by Johnson – Cook material model. More detailed failure and damage model such as GISSMO model should be used to model such instabilities accurately [39].

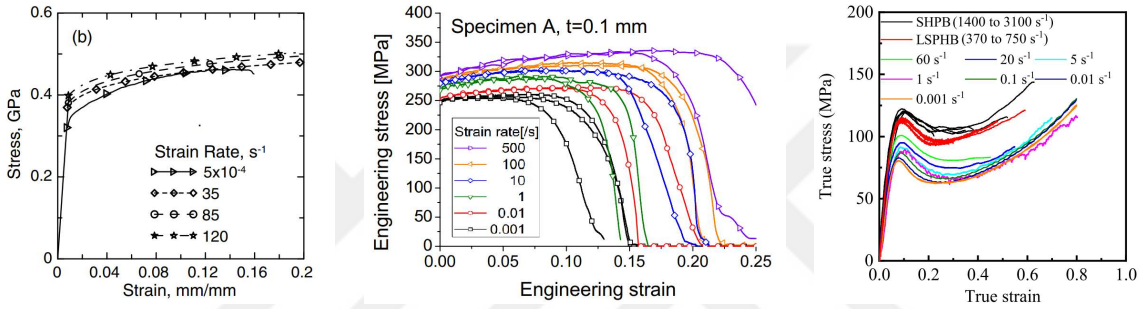

Figure 55: Experimental results from literature for AA6061-T6, OFHC Copper and Polycarbonate from left to right [40] [41] [42].

Figure 55 shows literature experimental results for materials used in this study under different strain rates. Comparing these results with experimental results given in section 4.2 a good match is observed. All literature results used a correction for the elastic region of stress data due to testing methods, in this study elastic region was not corrected to show the effect of wave propagation in the output bar. When yield strength of the materials are compared with the literature values, all results obtained from the testing system used in this study shows less than 10% error. This is an acceptable error for the purposes of this study.

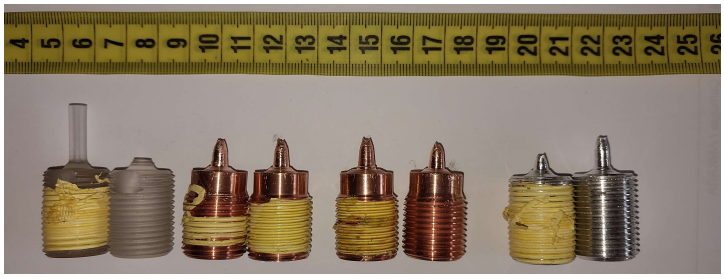

Figure 56: Tested specimens

5. CONCLUSIONS

In present study, an intermediate strain rate material testing device is designed, manufactured and its application with different materials are shown. In many different engineering applications, knowing and being able to model the intermediate strain rate response of a material is crucial. However, there are not many commercial testing systems that can provide that data. Testing system used in this thesis is used for obtaining the material response of AA6061-T6, OFHC Copper and Polycarbonate under intermediate strain rates. Results of these tests are given and compared to literature data. Overall error of experimental results was less than 10%. Additionally, numerical simulations are conducted with LS-DYNA software and numerical results are also compared to experimental results which showed a good match. Furthermore, repeatability of the system is shown by repeating tests. Therefore, it is shown that the intermediate testing device shown in this study has accuracy and repeatability.

Testing system is open to many improvements and in the future, many different materials can be tested under different strain rates using this testing system. Servo motor can be controlled to select the desired crosshead speed which would allow the users to change the strain rates. However, it should be kept in mind that with decreased motor rpm, maximum load allowed is also decreased. Slack adapter designs can be implemented to overcome this challenge. These adapters let the crosshead accelerate without pulling on the specimen before the test to increase strain rates.

Different types of specimens can be implemented to this device to observe failure and shear behavior. Additionally, different specimen interfaces can be used to gain a more robust strain signal. Threaded interfaces were not as efficient as desired. Noise levels seen in some of the experimental results can be reduced by modifications on supports and data acquisitions tools. Some modifications on the linear supports could make them better aligned, and make the specimen mounting process easier. Finally, DIC methods can be studied and applied to this system to better observe local deformations on the specimens.

System can also be used to conduct uniaxial compression tests under intermediate strain rates. However, the challenge of compression tests is that axial load keeps increasing during testing on the contrary to tension tests. This should be accounted for and maximum load allowed by the servo motor should not be exceeded.

6. REFERENCES

[1] January 2024. [Online]. Available: https://www.nuclear-power.com/nuclear-engineering/materials-science/material-properties/strength/. [Accessed 10 February 2024].

[2] Creative Commons Attribution, "Introduction to Aerospace Structures and Materials," 2023. [Online]. Available: https://ocw.tudelft.nl/course-readings/1-1-6-main-takeaways-on-stress-and-strain/. [Accessed 10 February 2024].

[3] M. A. Meyers, Dynamic Behavior of Materials, John Wiley & Sons, Inc., 1994.

[4] G. R. Johnson and W. H. Cook, "A constitutive model and data for metals subjected to large strains, high strain rates and high temperatures," *In Proceedings of the 7th International Symposium on Ballistics,* vol. 21., pp. 541-547, April 1983.

[5] Z. Chao, L. Jiang, G. Chen, Z. Q., N. Zhang, Q. Zhao, B. Pang and G. Wu, "A Modified Johnson-Cook Model with Damage Degradation for B4Cp/Al Composites," *Composite Structures,* vol. 282, no. 115029, 2022.

[6] H. Kolsky, "An investigation of the mechanical properties of materials at very high rates of loading.," *Proc. Phys. Soc.,* pp. 676-700, 1949.

[7] I. Rohr, H. Nahme, K. Thoma and C. Anderson, "Material Characterisation and Constitutive Modelling of a Tungsten - Sintered Alloy for a Wide Range of Strain Rates," *International Journal of Impact Engineering,* 2008.

[8] C. R. Siviour and J. L. Jordan, "High Strain Rate Mechanics of Polymers: A Review," *Journal of Dynamic Behavior of Materials,* pp. 15-32, 2016.

[9] R. W. Armstrong and W. S.M., "High strain rate properties of metals and alloys," *International Materials Reviews,* pp. 105-128, 2013.

[10] Y. Xia, J. Zhu, K. Wang and Q. Zhou, "Design and verification of a strain gauge based load sensor for medium-speed dynamic tests with a hydraulic test machine," *International Journal of Impact Engineering,* 2015.

[11] T. Bhujangrao, C. Froustey, E. Iriondo, F. Veiga, P. Darnis and F. Mata, "Review of Intermediate Strain Rate Testing Devices," *Metals,* vol. 10, 1 June 2020.

[12] Instron, "UNIVERSAL TESTING SYSTEMS," Instron, 2024. [Online]. Available: https://www.instron.com/en/products/testing-systems/universal-testing-systems. [Accessed February 2024].

[13] W. Cai, Z. Zhou, X. Qian, D. Cao, S. Li, L. Zhu and H. Hu, "Numerical Study on Ductile Failure Behaviours of Steel Structures under Quasi-Static Punch Loading," *Journal of Marine Science and Engineering,* vol. 11, p. 1197, 2023.

[14] V. Kamble, K. Shinde and J. Kittur, "Overview of Load Cells," *Journal of Mechanical and Mechanics Engineering,* vol. 6, no. 3, pp. 22-29, 2020.

[15] R. Watson, "Calibration Techniques for Extensometry: Possible Standards of Strain Measurement," *J. Test. Eval.,* vol. 21, no. 6, pp. 515-521, 1993.

[16] H. Konokman, M. Coruh and A. Kayran, "Computational and experimental study of high-speed impact of metallic Taylor cylinders," *Acta Mechanica,* vol. 220, no. 1, pp. 61-85, 2011.

[17] G. Gray, P. J. Maudlin, L. M. Hull, Q. K. Zuo and S. Chen, "Predicting material strength, damage, and fracture The synergy between experiment and modeling," *Journal of Failure Analysis and Prevention,* vol. 5, pp. 7-17, 2005.

[18] W. Chen and B. Song, Split Hopkinson (Kolsky) Bar, Springer Science+Business Media, LLC, 2011.

[19] P. Markovsky, J. Janiszewski, V. Bondarchuk, O. Stasyuk, D. Savvakin, M. Skoryk, K. Cieplak, P. Dziewit and S. Prikhodko, "Effect of Strain Rate on Microstructure Evolution and Mechanical Behavior of Titanium-Based Materials," *Metals,* vol. 10, 2020.

[20] B. Song, B. Sanborn, J. Heister, R. Everett, T. Martinez, G. Groves, E. Johnson, D. Kenney, M. Knight and M. Spletzer, "Development of “dropkinson” Bar for Intermediate Strain-rate Testing," *EPJ Web Conf.,* p. 183, 2018.

[21] M. Leblanc and D. Lassila, "Ahybrid technique for compression testing at intermediate strain rates," *Exp. Tech.,* vol. 20, pp. 21-24, 1996.

[22] R. Othman, P. Guégan, G. Challita, F. Pasco and D. A. LeBreton, "A modified servo-hydraulic machine for testing at intermediate strain rates," *Int. J. Impact Eng.,* vol. 36, pp. 460-467, 2009.

[23] M. Sutton, J. Orteu and H. Schreier, Image Correlation for Shape, Motion and Deformation Measurements: Basic Concepts, Theory and Applications;, Germany: Springer Science & Business Media: Berlin, 2009.

[24] T. Chu, W. Ranson and M. Sutton, "Applications of digital-image-correlation techniques to experimental mechanics," *Exp. Mech.,* vol. 25, pp. 232-244, 1985.

[25] R. Othman, The Kolsky-Hopkinson Bar Machine, Springer International Publishing AG, 2018.

[26] B. Lundberg and A. Henchoz, "Analysis of elastic waves from two-point strain measurement," *Exp. Mech.,* vol. 17, pp. 213-217, 1977.

[27] N. Yanagihara, "New measuring method of impact force," *Bull Jpn Soc. Mech. Eng.,* vol. 21, pp. 1085-1087, 1978.

[28] E. Jacquelin and P. Hamelin, "Force recovered from three recorded strains," *Int. J. Solids Struct.,* vol. 40, pp. 73-87, 2003.

[29] R. Othman, "Comparison of three methods to separate waves in the processing of long-time Hopkinson bar experiments," *Int. J. Mech. Eng.,* vol. 5, pp. 114-119, 2014.

[30] D. Casem and M. Zellner, "Kolsky bar wave separation using a photon doppler velocimeter," *Exp. Mech.,* vol. 53, pp. 1467-1473, 2013.

[31] H. Zhao and G. Gary, "A new method of wave separation for application to dynamic testing," *C. R. Acad. Sci. Paris,* vol. 319, pp. 987-992, 1994.

[32] H. Zhao and G. Gary, "A new method for the separation of waves. Application to the SHPB technique for an unlimited measuring duration," *J. Mech. Phys. Solids,* no. 45, pp. 1185-1202, 1997.

[33] J. Sun, K. Lee and H. Lee, "Comparison of implicit and explicit finite element methods for dynamic problems," *Journal of Materials Processing Technology,* vol. 105, no. 1-2, pp. 110-118, 2000.

[34] R. Furferi, Y. Volpe and G. Lapo, "Computer-aided design of new service doors for recreational vehicles," *International Journal of Mechanics,* vol. 9, 2015.

[35] M. Akbari and P. Asadi, "Dissimilar friction stir lap welding of aluminum to brass: Modeling of material mixing using coupled Eulerian–Lagrangian method with experimental verifications," *Proceedings of the Institution of Mechanical Engineers,* vol. 234, no. 8, pp. 1117-1128, 2020.

[36] LIVERMORE SOFTWARE TECHNOLOGY CORPORATION (LSTC), LS-DYNA Theory Manual, 2016.

[37] D. J. Littlewood, "Simulation of Dynamic Fracture Using Peridynamics, Finite Element Modeling, and Contact," *Proceedings of the ASME 2010 International Mechanical Engineering Congress & Exposition,* 2010.

[38] ATB Automation, "Linear Servo Actuator," 2024. [Online]. Available: https://atbautomation.eu/nl/. [Accessed 1 March 2024].

[39] J. Effelsberg, A. Haufe, M. Feucht, F. Neukamm and P. Du Bois, "On Parameter Identification for the GISSMO damage model," *12th International LS-DYNA Users Conference,* 2019.

[40] J. S. Kim and H. Huh, "Evaluation of the Material Properties of an OFHC Copper Film at High Strain Rates Using a Micro-Testing Machine," *Experimental Mechanics,* vol. 6, no. 51, pp. 845-855, 2010.

[41] P. Song, A. Trivedi and C. Siviour, "Mechanical response of four polycarbonates at a wide range of strain rates and temperatures," *Polymer Testing ,* no. 121, 2023.

[42] D. Zhu, B. Mobasher, S. Rajan and P. Peralta, "Characterization of Dynamic Tensile Testing Using Aluminum Alloy 6061-T6 at Intermediate Strain Rates," *Journal of Engineering Mechanics,* no. 137, pp. 669-679, 2011.